Inorganic Chemistry Communications 158 (2023) 111532

Contents lists available at ScienceDirect

Inorganic Chemistry Communications

journal homepage: www.elsevier.com/locate/inoche

Short communication

Development of tellurium/cerium bimetallic nanoparticles using biological method and their detection and degradation of keratin

M. Sindhu Devi [a], A. Muthuvel [b], S. Srinivasan [a,*], Abeer A. AlObaid [c], Ismail Warad [d,e], Basheer M. Al-Maswari [f]

[a] Department of Chemistry, Annamalai University, Chidambaram, Tamil Nadu 608002, India
[b] Department of Physics, Theivanai Ammal College for Women (Autonomous), Villupuram, Tamil Nadu 605602, India
[c] Department of Chemistry, College of Science, King Saud University, P.O. Box 2455, Riyadh 11451, Saudi Arabia
[d] Department of Chemistry, AN-Najah National University, P.O. Box 7, Nablus, Palestine
[e] Research Centre, Manchester Salt & Catalysis, Unit C, 88-90 Chorlton Rd, M15 4AN Manchester, United Kingdom
[f] Department of Chemistry, Yuvaraja's College, University of Mysore, Mysuru, Karnataka 570005, India

ARTICLE INFO

Keywords:
Bimetallic
TeCe
C. *Camphora*
XRD
Sensing
Keratin

ABSTRACT

In the present investigation, a novel eco-friendly synthesis of TeCe BNPs is fabricated from *Cinnamomum camphora-mediated* leaf extract. Biofabricated TeCe BNPs mediated by *C. Camphora* are characterized by various studies, such as UV–visible spectroscopy, XRD, SEM, HR-TEM, AFM, and XPS. The surface morphology of bioactive TeCe BNPs is visualized through SEM and AFM studies. The average particle size of TeCe BNPs is found to be 103 nm, with a zeta potential of 0.3, which confirms the stability and dispersive nature of BNPs. The decrease in absorption intensity with an increase in light irradiation reveals the primary degradation of keratin. FTIR studies confirm the formation of a disulfide band in the region of, 1115 cm^{-1}. Furthermore, an electrochemical biosensor based on *C.Camphora* mediated TeCe BNPs modified glassy carbon electrode was developed for the determination of keratin under optimal conditions. The biosensor exhibits a linear response in the potential range of 0.9–1.0 μm, with a limit of detection of 0.0562 μm and a detection limit of 4.8951E^{-4}.

1. Introduction

Keratin is a naturally available fibrous–structured protein that is the main constituent of corneous epidermal tissues in animals [1]. It belongs to the large family of structural proteins to form hair, wool calamus, pins, and antlers of any kind of animal with an elevated concentration of cysteine-containing 7–20% of the sum amino acid residue that forms inter and intramolecular disulfide bonds [2] it is also classified into alpha keratin and βkeratin based on the sub-coordinate construction of a protein. In alpha keratin, the alpha-helical –coils of type I (acidic) and type II (basic/Neutral) protein chains are coiled together to form elongated alpha helix filaments that form fibrils by interchain bonding, while β keratin is mainly built of βsheet [3]. The excessive count of disulfide bonds in the design of alpha keratin makes it insoluble and resistant to enzymatic lysis (Proteases) [4]. Keratin will contain more than 90% of the dry weight of the hair. The keratin in mammalian hair is less tough than the pleated sheet of β – keratin in feathers [5] (see Scheme 1).

A generation of keratin waste is carried out from meat industries in various forms, like chicken feathers, beaks, and the mixture of bone organs and hard tissue, and chicken feathers, which raise environmental pollution, as well as causes adverse effects on people's lives. A percentage of keratin protein debris, namely hair, horns, and rolls is discarded by leather industries and by Baber and hairstyle shops. To overcome this issue, various methods like recreation, landfilling, compositing, and mechanical grinding are used. In addition, recently diverse methods have been introduced, such as hydrothermal, chemical, enzymatic, and biological treatments to improve the digestibility of feathers [2]. Alternatively, a keratinase formation from *bacillus licheniformis PWD-1*, *B. licheniformis, bacillus pumilus F Hand*, *bacillus subtilis KD-N2, B. cereus*, *B. amyloloquefaciens*, *B, Megaterium, stenotrophomonas* SP.*D1 leuconostoc Sp*, *Pseudomonas microphilus*, as well as fungi like *trichophyton*, *Aspergillus flavipes*, etc. be reported. In addition, A.R. Birari et al utilized *stenotrophomonas* Sp. *AB 20 for* keratinolytic activity. The result of this study conveys greater than 87.3% fringe deterioration during 6 days using a submerged degradation process [6]. The study of

* Corresponding author.
E-mail address: chemssrinivasan@gmail.com (S. Srinivasan).

https://doi.org/10.1016/j.inoche.2023.111532
Received 7 August 2023; Received in revised form 19 September 2023; Accepted 29 September 2023
Available online 1 October 2023

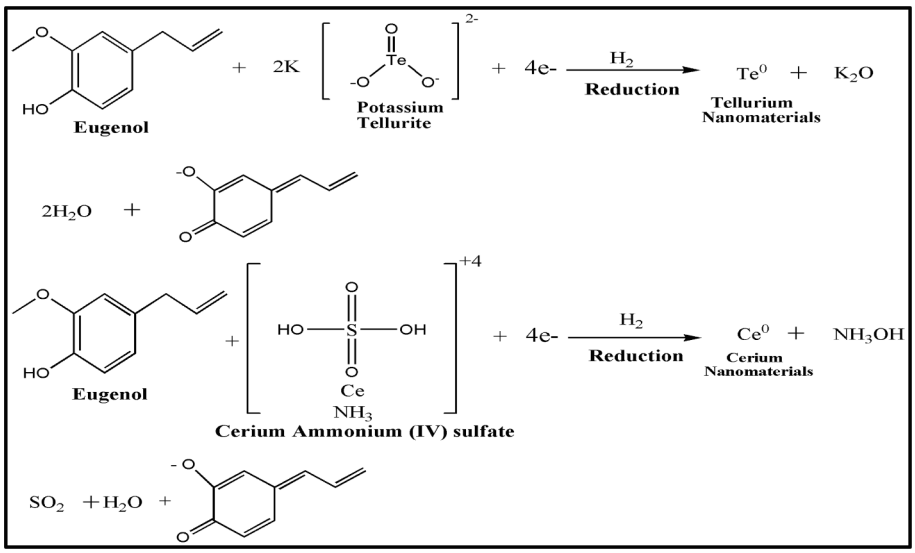

Scheme 1. General scheme for the method of synthesis of TeCe BNPs.

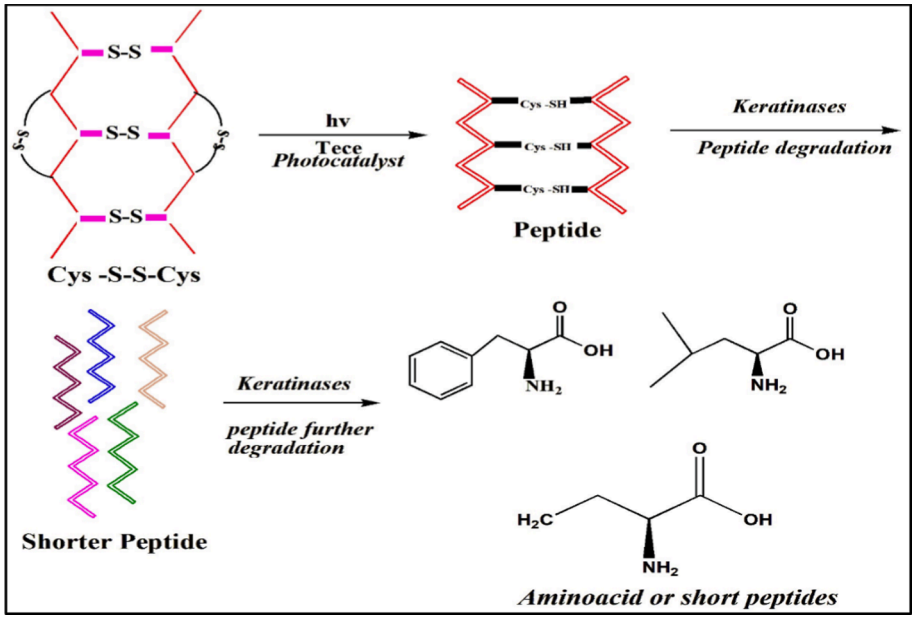

Scheme 2. Mechanism of degradation of keratin.

the photodegradation of keratin leads to significant changes in the physical, chemical, and mechanical properties of fibers [7]. Photolysis of wool keratin leads to the production of cysteine, cysteic acid, and limited oxidized cysteine species on UV – exposure at 254 nm [8]. Dinen Dshah et al studied the photochemical stability of therapeutic protein on light exposure, which leads to photo-oxidation of therapeutic IgG1mAb as per the ICH guidelines. Hence, exposure to light will make the CH_2 domain destabilized and will bring no major changes to the whole design of a protein [9]. Apart from many sources, keratin degradation is done by using a large variety of microorganisms *Bacillus licheniformis PWD-1* (Williams et al 1990, Lin et al 1992), *Fervidobacterium Pennavorans* (Friedrich, and Antranikian 1996), *Kocuria rosea LBP -3* (Vidal et al 2000, Bernal et al 2003), *Bacillus subtilis KS1* (Kim et al 2001,suh and lee 2001).*Bacillus pumilus*, *Bacillus cereus*, *Bacillus* Sp. *FK28* (Pissuwan and Suntornsuk, 2001), *Thermoanaerobacter* Keratinophilus Sp.*nov* (Riessen and Antranikian 2001), *Bacillus licheniformis K-508(Rozs et al 2001, Manczinger et al 2003)*, *Xanthomonas maltophilia POA −1* (De Toni et al 2002) have been reported [10]. Rania Ouertani et al isolated *bacillus halotolerans 4BC* (4BC strain) from tannery wastewater are incubated it on a keratin azure, calf hair, and plume meal agar plate. The result of studies shows almost 88% of the degradation of poultry plumes after 10 days of farming in feather powder bowl at p^H 8 and 370 convey the efficiency of keratin on bovine hair degradation compared to feather keratin [11]. Effective eco-friendly corruption of keratin by several keratinocyte fungal strains isolated from soil (*Fusarium* Sp.*1A*). A height loss of (71.10%) was obtained after incubation of *Fusarium* Sp.*1A* [12]. Zheng Peng et al proposed that the coordinative action of keratinase and sulfite through the degradation of feather waste leads to the production of amino acids and polypeptides [13]. A discarded waste from the leather and pelage industries in domestic sheepskin and wool was deteriorated by four freshly isolated *thermoactinomyces strains* and also compared with alkaline hydrolysis [14]. In this study, the decadence of keratin is done by using UBCH5 family members. On this basis, Ubc3 takes part in the decline of keratin IF proteins. Whereas, UBCH5a and –C were shown to prevent shear stress-mediated deterioration of the keratin IF peptide in human A549 cells. Hence, phosphorylation K8Ser −73 is

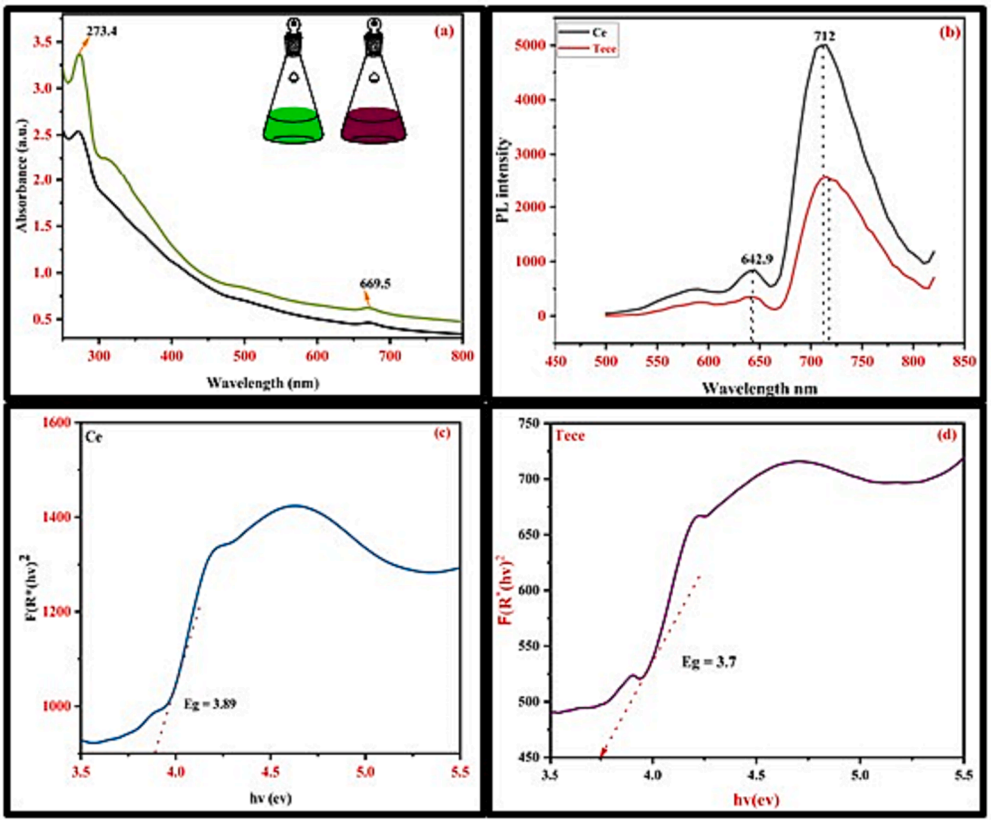

Fig. 1. (a) UV –visible spectra of TeCe BNPs (b) PL spectrum of TeCe BNPs (c) UV- DRS spectrum of TeCe BNPs (d) UV –DRS spectrum of Te.

responsible for the ubiquitination of keratin protein, followed by shear stress in A549 [15]. A study on pathogen community-based demolishment of keratin by using four soil isolates: *Stenotrophomonas rhizophila, Xanthomonas retroflexus*, *Micro – bacterium oxydans, and paenibacillus amylolyticus*. The result suggests an acceleration in keratin degradation rates on cocultured and monoculture of *X. Xetroflexus* microorganisms, respectively [16]. Mukesh Sharma tested the invitro environmentally - friendly keratin by clinical insulation of dermatophytes and soil fungi. The result reveals that human fiber had an excessive rate of keratin destruction (56.66%) by colorization of *C. Indicum*, *M. Gypseum,* and *T. Verrucosum* which was an extreme derogation (49.34%) from beast hair, showed a significant role of fungi in the biodegradation of keratin substrates [17]. A large variety of microorganisms such as *paenarthrobacter nicotinovorans* (Sone et al., 2015) *Nocardiopsis Sp TOA -1* (Mitsuiki et al., 2004) *Streptomyces albidoflavus* (Ma et al., 2017), *streptomyces fradiae* (Li et al., 2007) *Parengyodontium album* (Ebeling et al 1974, Jany et al 1986), *Stenotrophomonas maltophilia* (Fang et al., 2014) *Stenotrophomonas maltophilia* (Fang et al., 2014), *Fervidobacterium pennivorans* (Friedrich and Antranikian 1996, Kim et al 2004) *Thermoactinomyces* Sp. *CDF* (Wang et al 2015) *Bacillus licheniformis* (Ramnani and Gupta 2004), *Bacillus subtilis* (Gupta and singh, 2013) *Bacillus amyloliquefaciens* (Gupta and singh, 2013), *Bacillus pumilus* (Fellahi et al 2016), *Bacillus cereus* (Ghosh et al 2009), *Bacillus halodurans JB99* (Shrinivas and Naik 2011), Meiothermus taiwanensis (Wu et al 2012), *Stenotrophomonas maltophilia* (Jankiewicz et al 2016), *thermoactinomyces* Sp.*YT06* (Wang et al 2017), *Trichophyton benhamiae(Jousson et al 2004)*, *Trichophyton rubrum, Onygena Corvina*(Jousson et al 2004,Huang et al 2004),*Microsporum canis* (Descamps et al., 2002) *Aspergillus niger* (chen et al 2015,Jarai et al 1994),*Trichophyton mentagrophytes* (Yohko et al 2014), *Trichophyton rubrum* (Monod et al., 2005,Zaugg et al., 2008),*Fervidobacterium islandicum* (Kang et al 2020), Onygena corvina (Huang et al 2015), *Psuedomonas aeruginosa* (Sharma and Gupta, 2010), *Geobacillus stearothermophilus* (Gegeckas et al 2015), *Trichophyton rubrum* (Zaugg et al 2009,2008), Fervidobacterium islandicum(Kang et al 2020), *Trichophyton rubrum* (Monod et al 2005) *Onygena corviae* (Huang et al 2015), *Streptomyces fradiae* (Wu et al 2010), *Onygena corvina* (Huang et al 2015), *Trichophyton rubrum* (Monod et al 2005), *Fervidobacterium islandicum* (Lee et al 2015), *Fusarium oxysporum* (Chaya et al 2014), *Microsporum canis* (Brouta et al 2002), *Onygena corvina* (Huang et al 2015), *Fervidobacterium islandicum* (Kang et al 2020*),* be reported [3]. Hence, the microbial degradation of keratin will result in various applications for several purposes as feed, fertilizer, detergents, and leather, as well as pharmaceutical and biomedical applications [10] (see Scheme 2)

In the present study, *C. Camphora-mediated* TeCe BNPs were utilized for keratin degradation. Further characterized by using various studies such as XRD, SEM, FTIR, HR-TEM, EDX, etc. In addition, bioactive TeCe is utilized for keratin degradation to verify the photocatalytic behaviour of BNPs. Sensing activities of TeCe BNPs are tested by using cyclic voltammetry through various sensors like tryptophan, methyl uracil, and uric acid.

2. Experimental

2.1. Materials

All the chemical substances used in the method were A.R Grade and obtained from the Sigma Aldrich branch in India. Filtration was done using the Whatman 40 filter paper. Chemicals such as Ammonium cerium sulphate, Potassium telluride (7790-58-1), and Keratin (57-88-5), were purchased from Subra Scientific Store, Pondicherry, India. Methanol (26-67-56-1) was bought from S. Devi Chand & Co (chem.) Private Limited. Chennai, India. Further, the chemicals Ferric chloride (775-08-01), Sodium chloride (764714-5), Potassium chloride (7447-40-7), Tryptophan (73-22-3), Uric acid (69-93 -2), Methyl uracil (626-48-2), Potassium Ferro cyanide (14459-95 -1) were purchased from nice chemicals Pvt. Ltd Cochin, India.

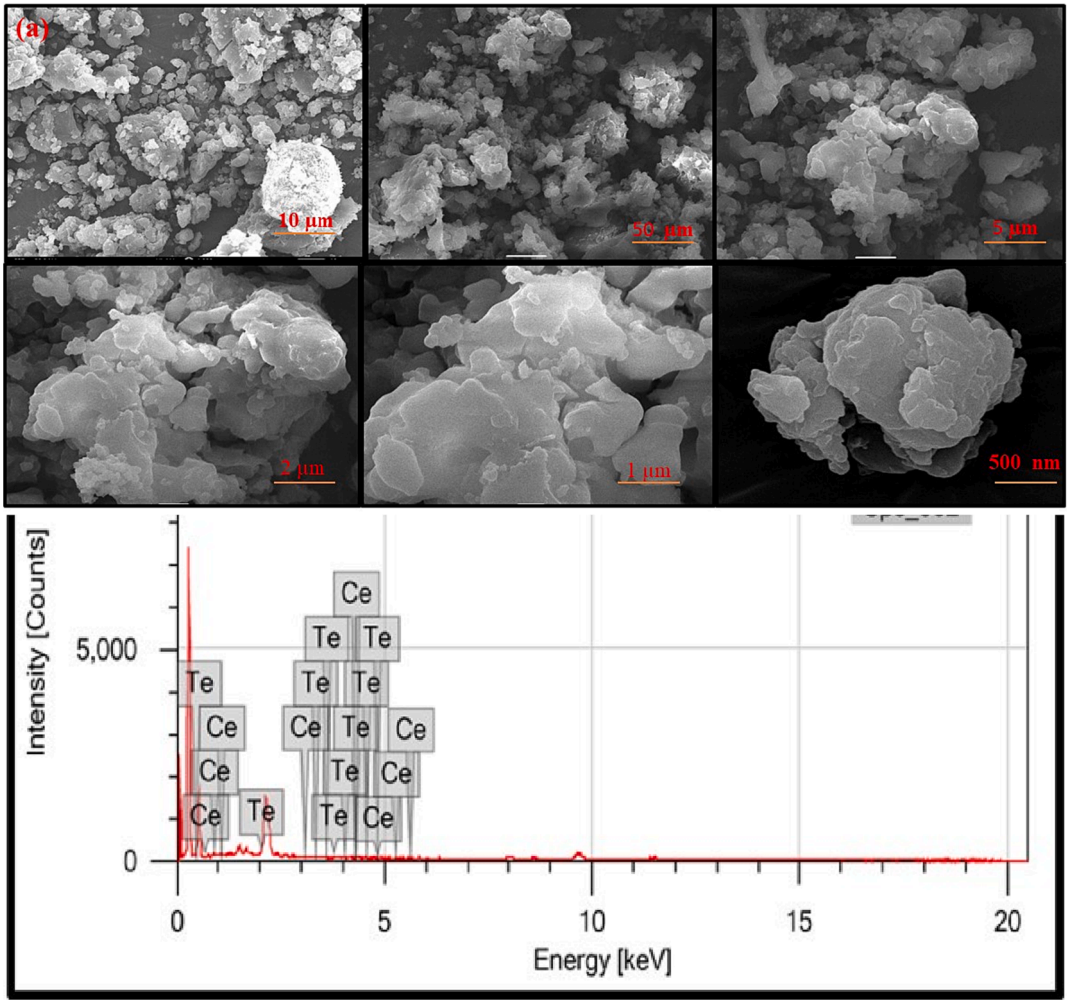

Fig. 2. (a) SEM image (b) EDX spectrum of biosynthesized TeCe BNPs.

2.2. Preparation of leaf extract

A colloidal suspension of TeCe BNPs is prepared by following a two-step procedure. Initially, a plant extract is prepared using approximately 30 g of finely powdered *C. Camphora* leaf. The extracting solvent (Methanol) in a 1:10 ratio was added to a conical flask. It was stirred for about 30 min at 64 °C. As a result, the plant components in C. *Camphora* extract were removed. Further, the filtrate was separated using a rotary evaporation process for solvent separation. Finally, plant extract acquired from the rotary evaporation process was adjusted to P^H – 9 using sodium hydroxide solution and used as a reducing agent in biosynthesis [18].

2.3. Synthesis of TeCe bimetallic nanomaterial

Fabrication of TeCe BNPs was carried out by using a methanol extract of *C. Camphora* leaf extract obtained from plant extract preparation at P^H - 9. Potassium tellurite (200 µg/mL) and Ammonium cerium sulfate (50 µg/ML) solution were dissolved in 100 mL of the aqueous solution in an Erlenmeyer flask. The flask was stirred in a magnetic stirrer, followed by slow addition of plant extract at room temperature (37 °C) for 3hr and incubated for 78 hr. The colour change of the solution confirmed the formation of TeCe BNPs. Further, the obtained nanoparticle in colloidal suspension has been separated by a centrifugation process, and a core–shell form of Bimetallic nanoparticle was Stabilized by some of the phenolic components and natural polymer in plant products. UV – Visible spectra were used to identify the formation of NPs utilizing a Shimadzu UV–1650 Pc Spectrophotometer Japan, East Asia) operated at a resolution of 0.5 nm [18].

2.4. Evaluation of photocatalytic activity TeCe BNPs

Photocatalytic activity of TeCe BNPs is tested using the UV photoreactor 250MWT at different time intervals (2 –8hrs). In this experiment,50 mL of 20 ppm keratin solution at P^H – 7 is pipetted into a degradation tube and labeled 'O'. The Photocatalyst (TeCe) was mixed with keratin solution and ultra-sonicated for 15 min to obtain a uniform dispersion of BNPs. Further, a dark reaction is carried out to attain adsorption–desorption equilibrium between keratin and the catalyst (TeZr BNPs). The remaining solution was labeled as A and irradiated using the Herber Photo reactor at a different time interval (1–2 h). Finally, the concentration of the test solution after light irradiation was determined using a UV -spectrometer at 200–800 wavelength [32].

2.5. Electrochemical measurement

In this experiment, the measurement was conducted using a conventional three-electrode cell, where an electrode, a platinum wire, and a glassy carbon electrode (GCE, 3 nm in diameter) modified by catalyst were used as the reference electrode, counter electrode, and working electrode respectively. After being carefully cleaned, the sample was coated on the surface of the GCE with a load of approximately 4 µg. The cyclic voltammetry curves were measured by using an electrolytic solution at room temperature [19].

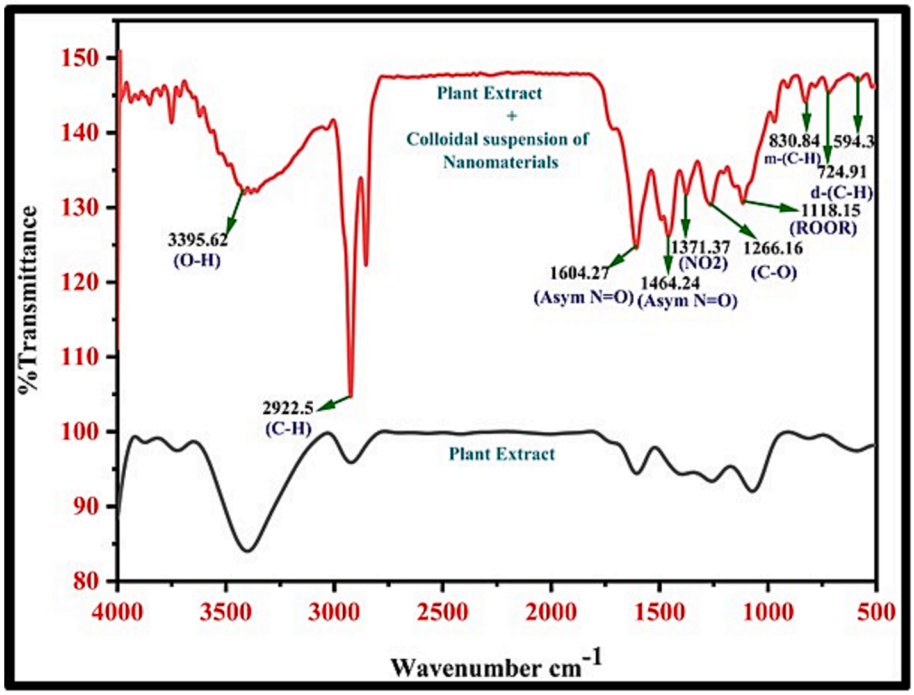

Fig. 3. FTIR spectrum of TeCe BNPs.

2.6. Characterization

UV–visible spectrum of the reaction mixture over a wavelength of 200–800 nm at different time intervals (Shimadzu UV−1650 pc Spectrophotometer) operated at a resolution of 0.5 nm at Annamalai University Chidambaram.

UV - DRS of Biosynthesized TeCe BNPs was taken with UV−3600 Shimadzu Spectrometer using $BaSO_4$ as the Standard in wavelength 800–200 nm at Annamalai University Chidambaram.

The X-ray Diffractometer system operated at a voltage of 40Kv and a current of 30 mA with Cukα radiation in Θ- 2 Θ configuration in the scan range 5.0–8.0. The X-ray intensities have been noted from 10 to 80 of 2 Θ angles at Karunya University, Coimbatore.

Surface morphology and Size of BNPs were analysed by HR – TEM using an FEI Techni G2 2505 –Twin at 200kv using a LeB6 or W emitter. It operated with 25X – 1030Kx magnification at Madurai Kamaraj University, Madurai.

The surface morphology and size of the purified TeCe BNPs were studied with scanning electron microscopy (SUPRA55 –CAROZEISS) operating at 20kv. Energy dispersive spectroscopy analysis was conducted with the same instrument for constituent analysis of the sample at Annamalai University, Chidambaram.

Fourier transforms infrared (FTIR) Spectroscopy for the BNPs with plant extract was recorded at 5 a.m. Perkin Elmer Spectrometer in the wavelength range of 8,300–350 cm^{-1} with a resolution of 0.5 cm^{-1} at Pondicherry University, Puducherry.

The particle size measurement of biosynthesized TeCe BNPs from 0.3 mm diameter to 5 μm is carried out using 90° degree scattering optics. The zeta potential of colloids and nanoparticles is measured using patented M3 –PALS technology using a He –Ne Laser at 633 nm using 10 mV. The temperature range extension option is 120 at Pondicherry University, Pondicherry.

AFM microscopy (Park N x10 S1CM) was applied to observe the morphology and surface topography of the BNPs using tapping mode with an RTESP tip. The resonance frequency of the tip was 281.33 kHz and the scanning range was 2. 0 μm at PSG University, Coimbatore. Cyclic voltammograms (CV) curves were obtained using a CH1600C electrochemical analyzer (CH instrument, Shanghai, China) at Annamalai University, Chidambaram.

3. Result and discussion

3.1. UV–visible spectroscopy

The colloidal suspension of bioactive TeCe BNPs before and after incubation at 37 °C for 84 hr under normal experimental conditions was illustrated (Fig. 1a). The reduction of Te(IV) Ce(III) by *C. Camphora* mediated TeCe detected by the black precipitate in the bio aliquots indicates the reduction of tellurium – cerium to TeCe BNPs. Hence, the conversion of green to black colour conforms to the formation of *C. Camphora-mediated* TeCe BNPs. The colloidal suspension of TeCe BNPs was prepared using a two-phase system by centrifugation. A UV – visible spectrum of TeCe reveals the absorption peak at 273,625 nm, which conforms to the surface Plasmon resonance peak of core–shell TeCe BNPs [20]. The band gap energy of TeCe BNPs is calculated by Tau's plot based on the kubelka – Munkfunction using the reflectance data. The kubelka Munk equation function is given as $F(R) = (1 - R)/2R$. The band gap energies of Ce and TeCe BNPs are 3.8 and 2.5 ev, respectively. They are obtained by plotting Tau's function $F(R*(hv)^2$ with $n = 2$ upon photon energy (ev), as illustrated in (Fig. 1c, d). The result of this study reveals the smallest band gap energy for TeCe BNPs compared to monometallic Ce, suggesting that the combination of Te with Ce will resist more size reduction due to the quantum confinement effect [21].

3.2. SEM analysis

An SEM image of TeCe BNPs presented the shape and size of the biosynthesized TeCe BNPs at different magnifications. The surface morphology of green fabricated TeCe BNPs in aggregated form is given below (Fig. 2a). The aggregated form of TeCe BNPs is due to the drying process observed. Observation of surface morphology at four different magnifications 10 μm, 5 μm, 2 μm, and 1 μm using 20 k reveals that BNPs were scaled in nanometres. An EDX graph (Fig. 2b) of biosynthesized TeCe BNPs displays the presence of Tellurium and cerium elements. The Lack of any other elements indicates the formation of

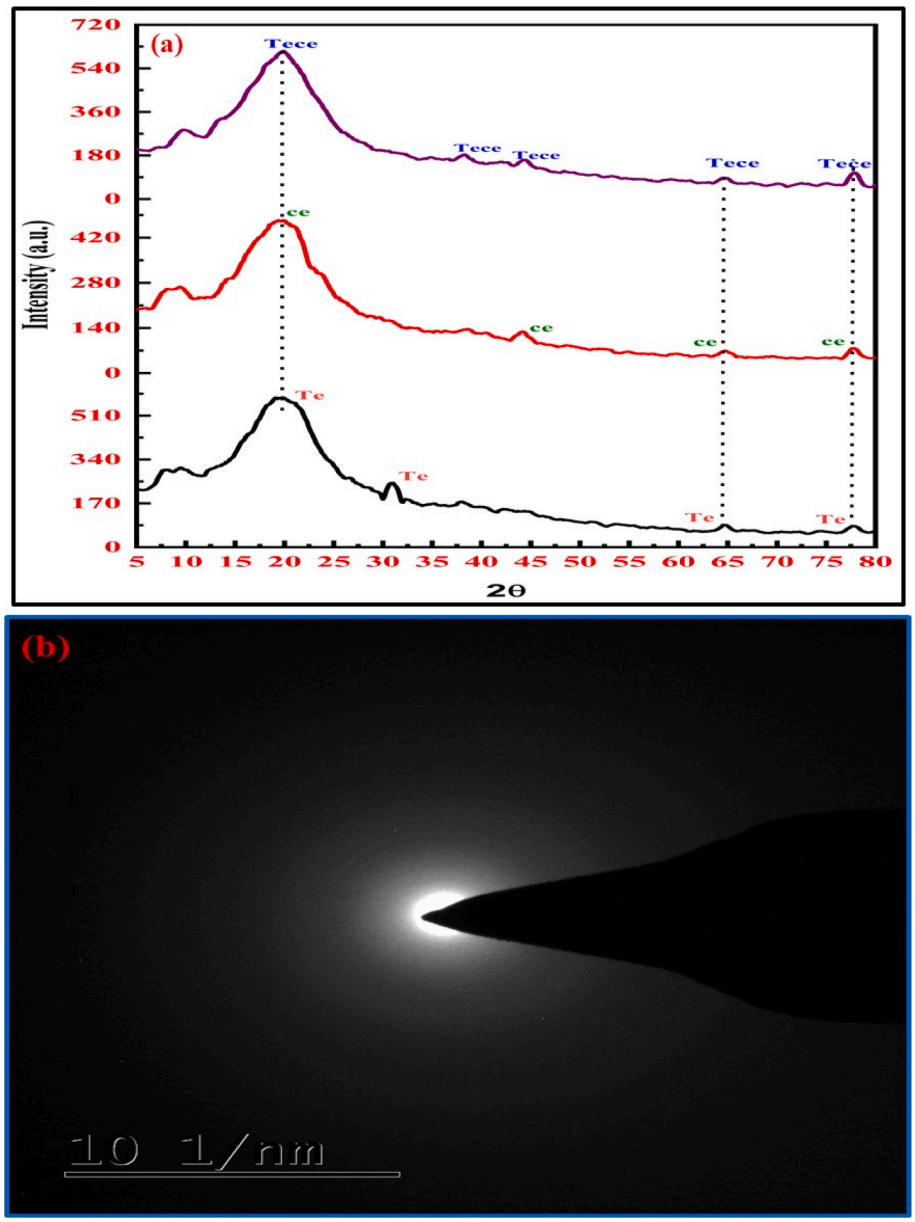

Fig. 4. (a) XRD image (b) SAED pattern of biosynthesized TeCe BNPs.

highly pure biosynthesized BNPs [21,22].

3.3. FTIR analysis

The FTIR spectrum of *C.Camphora mediated* TeCe BNPs in the range of 400–4000 cm^{-1} was taken for colloidal suspension of biosynthesized camphor-mediated Tece BNPs by the modified pechini method was obtained at p^H 9 without heat treatment. Fig. 3 shows the IR spectra of Biosynthesized Tece BNPs. Spectra show a large band at around 400–600 Cm^{-1} revealing the vibration mode of tension of TeCe BNPs, which conforms to the coexisting form of an organic compound with TeCe BNPs. In addition, the large band at around 3395.62 corresponds to the O–H stretching and bending mode of H_2O molecules at the surface of BNPs. Further, the appearance of stretching frequency peaks of C–H, C = O, and C = C, in the region of 2924.7, 2854.0, and 1460.2 that conforms to the coexisting form of an organic compound in colloidal suspension indicates the presence of a capping and stabilizing agent along with NPs [23].

3.4. XRD analysis

The amorphous nature of Biosynthesized Te, Ce, and TeCe BNPs has been investigated using the XRD technique. The PXRD pattern of Biosynthesized monometallic Te, Ce, and TeCe BNPs using *C.Camphora* leaf extract is shown in Fig. 4a. In the XRD pattern, the most prominent characteristic peak at 2θ–19.7 corresponds to planes (1 0 0) of TeCe, respectively. It indicates the formation of amorphous, bioactive BNPs. The appearance of poorly resolved peaks for Te and Ce NPs indicates the amorphous phase of nanoparticles. Further, the addition of a small amount of cerium on tellurium leads to the appearance of a broad peak at 2θ–19.7 (1 0 0) due to the aggregation of TeCe BNPs. However, it was noticed that a combination of tellurium with cerium in a 1:1 ratio would result in a lack of diffraction and a peak shift that would reveal the stability of BNPs (Fig. 4b). The result agrees with the reported literature from Sindhudevi et al who reported the production of camphor-mediated amorphous Tese nanostructure. In the SAED pattern, the absence of a diffraction pattern and the formation of diffused rings will directly conform to the amorphous phase of BNPs [18].

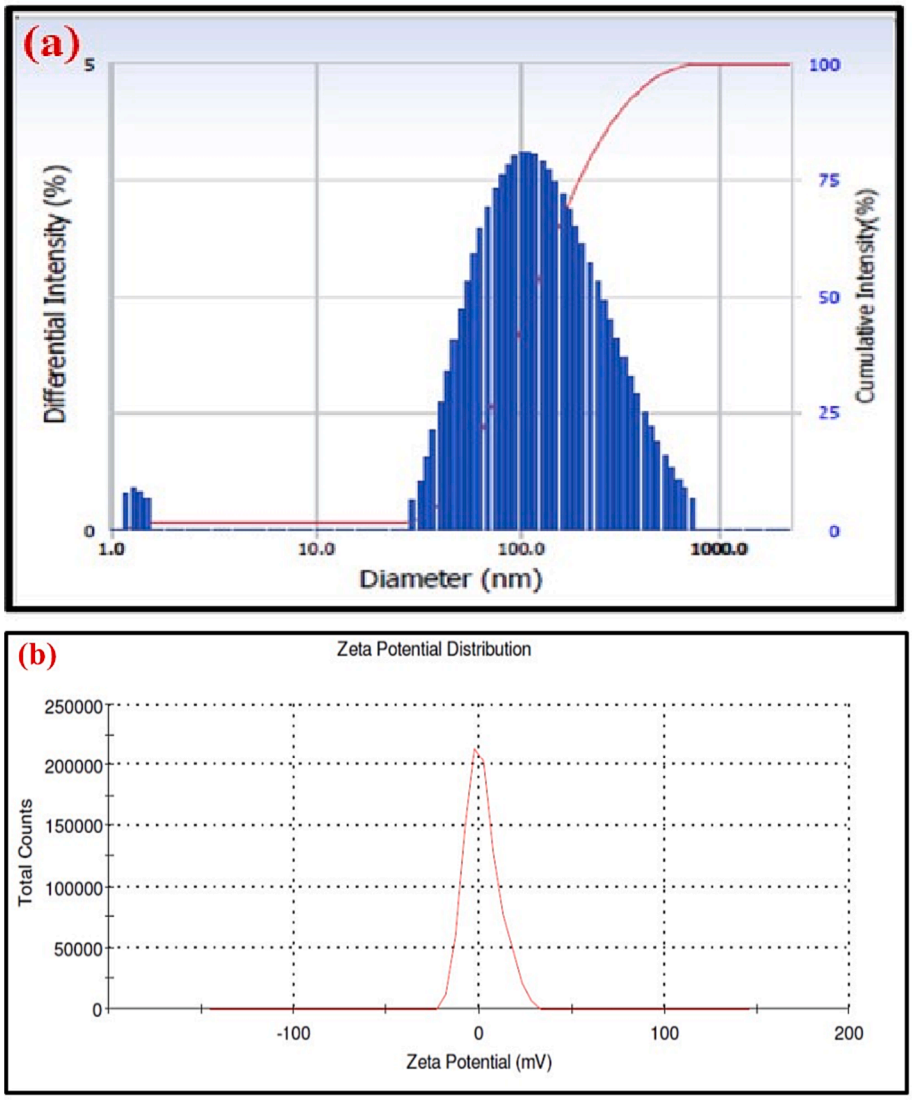

Fig. 5. (a) The hydrodynamic diameter of camphor-mediated TeCe BNPs (b) Zeta potential value of TeCe BNPs.

3.5. DLS analysis

The average particle size of TeCe BNPs was measured by the DLS technique. The plot of Size distribution against the differential intensity graph is represented in (Fig. 5). The average size of the bimetallic nanoparticle TeCe was found to be 103 nm. The large size of green synthesized TeCe BNPs is due to the hydrodynamic coating of TeCe BNPs. The zeta potential provides information regarding the surface charge and stability of Bioactive TeceBNps.The zeta potential of the BNPs was found to be −21 mV, showing that the strong electrostatic repulsion between the Nanoceria and other ionic species within the solution will conform to the stability and dispersive nature of BNPs. Hence, the rich source of alkaloids and terpenoids is responsible for the reduction of metal ions and their efficient stability [24].

3.6. AFM analysis

AFM image was used to visualize the high-quality surface morphology and uniformly distributed form of TeCe BNPs in 2D and 3D dimensions. Fig. 6a&b illustrates the 2D and 3D images of TeCe BNPs. The surface area of TeCe BNPs is found to be 8558, 8296, 8482, 8677, with a surface roughness of 2.6450, 1.938, 2.07091, 2.22235 nm and a root mean square roughness of 3.8666, 2.78579, 3.42887, 3.37965 for the particle at 35, 24, 32 and 28 nm, respectively (Fig. 6c). Hence, increases in surface area with increases in surface roughness due to decreases in particle size are observed (Table 1) [25].

3.7. XPS analysis

XPS is a sensitive technique for determining the conformation and oxidation properties of BNPs. (Table 2) lists the binding energy and FWHM value of BNPs. A formation of C, O, and N peaks in the spectrum indicates the organic materials that are responsible for keeping the particle in a green solution. Whereas the Appearance of C1s and O1s peaks at a binding energy of 288 ev and 535 eV, respectively, the –COO group is assigned. The Te3d and Ce3d signals were characterized by spin–orbit doublets Te3d5/2, Te3d3/2 Ce3d5/2, and Ce3/2, which were separated by 10ev.The curve fitting of the Te3d, Ce3d signal shows the presence of two peaks at binding energy 576.1, 576.3, 881, 881.4, assigned to the metallic and oxidation state of Tellurium cerium BNPs. Further, in the deconvolution of Te3d, the Ce3d peak is cleaved into two peaks at Binding energy of 531ev, and 312 ev respectively, conforming to the oxidation of Tece BNPs [26]. Fig. 7. (a) (i) A survey scan spectra of camphora mediated TeCe BNPs (ii) Te (ii) Ce (iii) O1s (iv) C1s (b) Deconvolution spectra of (i)Te (ii) Ce BNPs (iii) O1S (iv) C1S.

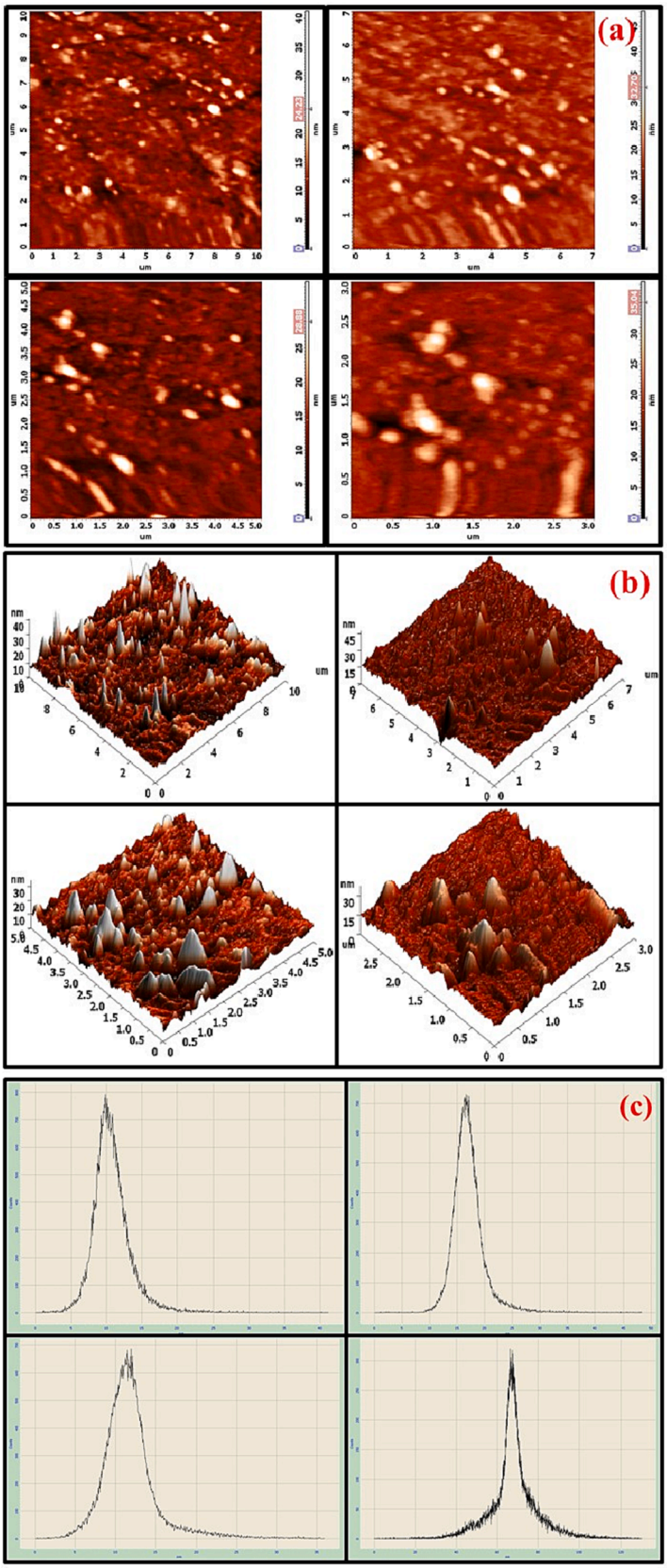

Fig. 6. (a) 2D topography (b) 3D image of *Cinnamomum camphora* mediated TeCe BNPs at different regions (24–35 nm).

Table 1
Surface area, surface roughness, and particle size of TeCe BNPs.

Nanomaterials	Particle Size nm	Surface areaμ2/m	Surface roughness nm	Root mean square nm
TeCe BNps	35	8558	2.6450	3.8666
	24	8296	1.938	2.78579
	32	8482	2.07091	3.42887
	28	8677	2.22235	3.37965

Table 2
Binding energy, FWHM with TeCe BNPs surface area.

Element	Binding Energy (ev)	FWHM	Area
Te3d	586.78	0.83	176,645
Ce3d	880.9	2.195	74093.4
C1s	288.12	2.24	3336.64
O1S	535.58	3.19	−6744.1

3.8. HR –TEM analysis

A particle size analysis of TeCe BNPs and its surface morphology was studied by TEM analysis. HR –TEM analysis of biosynthesized Core–shell TeCe BNPs is shown in (Fig. 8a). A core–shell form of TeCe BNPs was observed at a distant nanoscale range (10,5nm) on higher magnification. The morphology of TeCe BNPs was uniform, and spherical, with an average size of 24–35.5 nm on a scale of 15 to 45 nm, a Mean of 29.261, and a standard deviation of 7. 246. It has been similar to Oleo Europaea, Honey-mediated CeO_2, and lesser than Moringa Oleifera L extract (Fig. 8b). The micrograph analysis of fresh core–shell TeCe BNPs shows that a nanoparticle that is nearly uniform in spherical shape and well distributed on the surface will conform to the amorphous phase of TeCe BNPs. The particle size of TeCe BNPs in deionized water was calculated to be higher (1 0 3) compared to HR –TEM. The d spacing value was recorded as 4.5, corresponding to the plane (1 0 0) of ceria. The result of this study reveals a smaller particle size than the DLS study, due to the hydrodynamic coating of BNPs observed [27].

3.9. BET analysis

The surface area determination of Tece BNPs is accomplished utilizing a BET study. (Brunauer – Emmett Teller). The N2 adsorption–desorption isotherm and Barrett – Joyner – Halendu (BJH) pore size distribution plot of Tece BNPs are shown in (Fig. 9). The surface area, pore diameter, and total pore volume of the BNPs are 0.2614 cm^3 (STP) g-1), 1.0882, 3.0948E-^{04} [cm^3g^{-1}] respectively. [16,28]. Table 3 Pore diameter, specific surface area, and pore volume of TeCe BNPs.

4. In vitro way of degrading keratin

4.1. TLC (Thin-layer chromatography)

The thin layer chromatogram of various distributed molecular masses obtained in keratin degradation on light irradiation is illustrated in (Fig. 10). Observation of spots at the different regions for catalyst-loaded (TeCe BNPs) keratin after 1hr and 2hr of light irradiation confirms the formation of small oligopeptides. Further, the lack of movement of spots for blank keratin reveals the stability of keratin towards irradiation [29].

4.2. UV –Visible spectrum of Keratin

The ultraviolet–visible spectrum of keratin in the presence and absence of Photocatalyst TeCe is shown in (Fig. 11 a,b). The maximum absorption peak at 207 with intensity 3.6 for blank and 3.3 for keratin with the catalyst at 210 nm is obtained. Formation of the peak at 210 with decreases in intensity on increases in light irradiation after 2hr time intervals is observed. Hence, a depletion and shift in peak towards higher wavelength (2 1 0) for catalyst containing Keratin (2hr) on irradiation but not for blank keratin suggests the degradation efficiency of TeCe BNPs towards light irradiation [29,30,31].

4.3. FTIR analysis

FTIR spectrum of commercially available keratin before and after degradation through the utilization of camphora mediated TeCe BNPs are displayed in (Fig. 12a,b). The absorption band at 3446.5 cm-1 assigns the stretching vibration of O–H and N–H in amino groups and water molecules. The band at 2063.8 cm-1 is attributed to the symmetrical CH_3 stretching' frequency of the C = O absorption band appearing at 1635.3 cm-1. On the other hand, a stretching frequency peak at 3446.5 cm^{-1} indicates the α - helix. Further, the band at 1635.3 cm^{-1} shows the combined form of α - helix and β- sheet. Whereases, the Formation of the disulfide band in region 1115 cm^{-1} conforms to the degradation of keratin. The band at 616 cm^{-1} assigns the stretching vibration of VC-S, and the rocking vibration S–H band at 800–900 cm^{-1} indicates sulfur compounds [6,29,30,31].

4.4. SEM analysis

Morphology analysis of the keratin powder before light irradiation of the keratin solution has been investigated using SEM analysis. (Fig. 13a) illustrates the morphology of keratin powder before irradiation. On comparing images a and c, A will visualize the laminar and irregular plate-shaped structure, and B shows some crystalline form of keratin before light irradiation [12,31].

4.5. HR–TEM analysis

The surface morphology of Cinnamomum camphora-mediated TeCe-loaded Keratin powder after light irradiation has been predicted. (Fig. 13b) shows the morphology of keratin after light irradiation using a TeCe catalyst. The structure of keratin after irradiation is non–uniform, and a distorted form of particles has been observed at different magnifications, leading to stress and strain that could be suitable for photochemical transformation [12,31].

4.6. DLS analysis

Measurement of the differential intensity of reflected light indicates the particle size distribution of keratin obtained after 1hr and 2hr irradiation. (Fig. 14) elucidates the medium-size particle size in a range from 75−100 nm, intimately describing the degradation of keratin. However, blank keratin with a catalyst loaded on light irradiation will contain small particles in the higher area of 75–100 nm assigned to small oligopeptides and amino acids, confirming the conversion of polypeptides into small amino acids and oligopeptides [31].

4.7. HPLC – (High-performance liquid chromatography)

The degradation of standard keratin before and after irradiation was analyzed by the HPLC method. The retention time for standard keratin is similar to the literature reported. After 2 h of light irradiation, the formation of a new peak after peptide degradation leads to amino acids at 3.18, 4.376, and 8.743. (Fig. 15). HPLC Chromatogram of (a) Blank keratin and (b) HPLC chromatogram of keratin which was obtained after a 2hr irradiation. A chromatogram product obtained after 1 h of irradiation reveals the degradation of keratin [13].

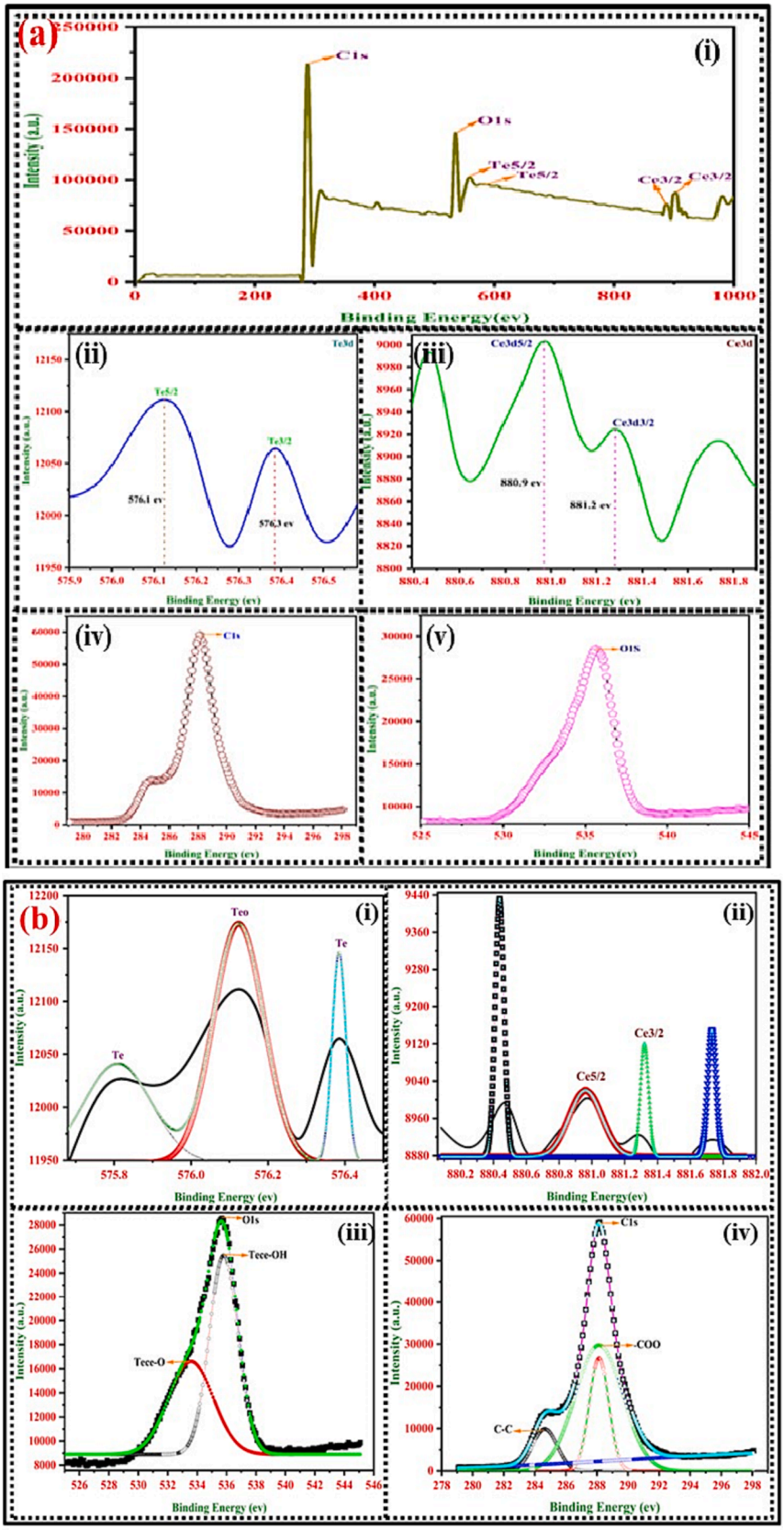

Fig. 7. (a) (i) A survey scan spectra of *camphora* mediated TeCe BNPs (ii) Te (ii) Ce (iii) O1s (iv) C1s (b) Deconvolution spectra of (i)Te (ii) Ce BNPs (iii) O_{1S} (iv) C_{1S}.

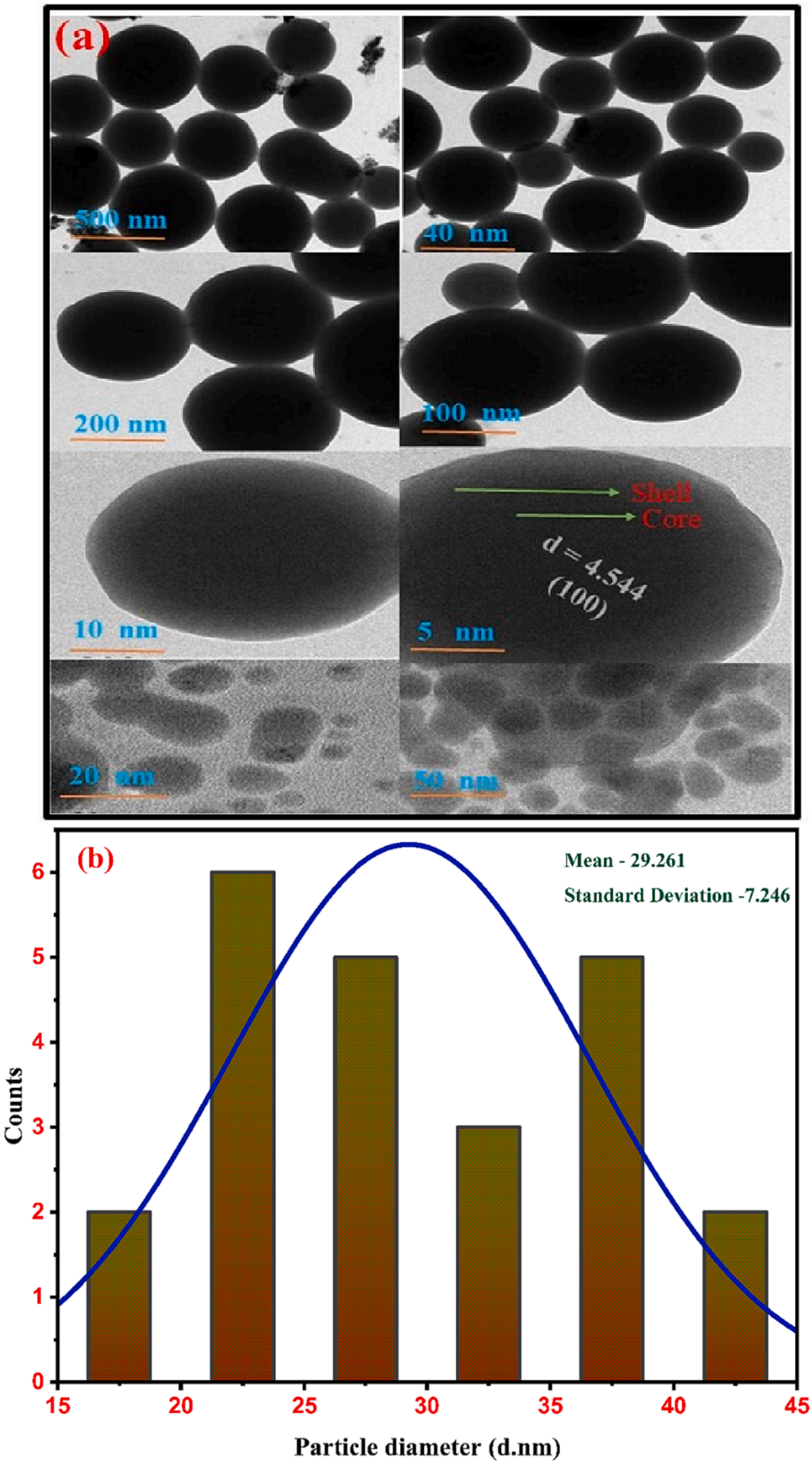

Fig. 8. (a) HR- TEM image of TeCe BNPs at different magnifications (b) particle size distribution.

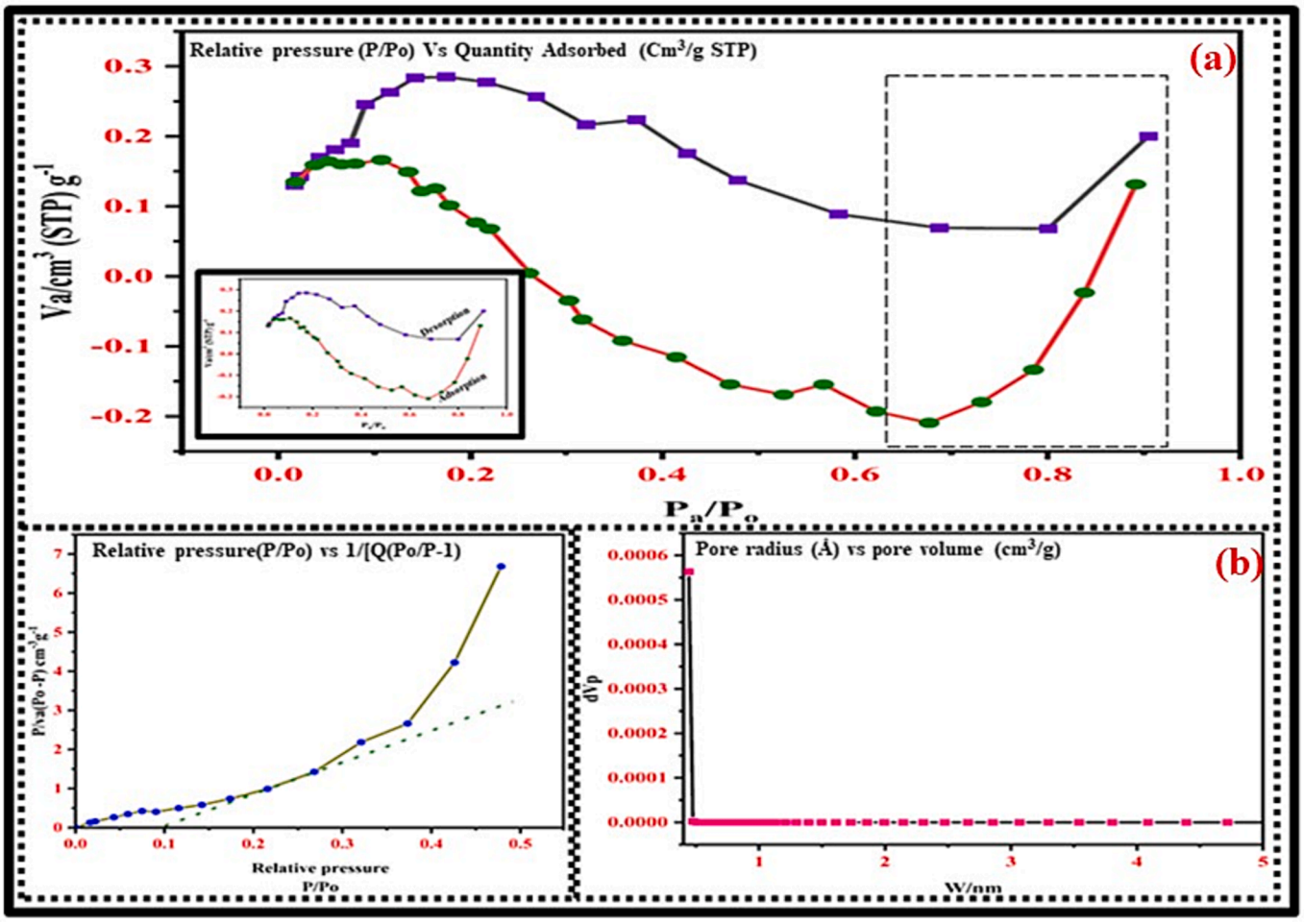

Fig. 9. (a) N2 adsorption–desorption isotherms of the Bio-synthesized TeCe BNPs (b) BJH size distribution of TeCe BNPs.

Table 3
Pore diameter, specific surface area, pore volume of TeCe BNPs.

parameter	Range
Vm-specific surface area	0.2614 [cm3 (STP) g^{-1})
Concentration C	40.956
Mean pore diameter	1.0882
as BET	1.1375E + 00 [m^2g^{-1}]
Total pore volume	3.0948E^{-04} $^{3}_{[cm\ g^{-1}}$

4.8. Mass spectrum of keratinase product

HR – mass analysis of blank keratin and its product, which was obtained after 2 h of light irradiation, was used to identify the keratinase product (Fig. 16). HR-mass spectrum of (a) blank keratin (b) HR-mass spectrum of keratinases product after 2hr of light irradiation. The molecular ion peak at *m/z* ratio of citrulline (176.065), Lysine (329.14), Valine (177.068), Hydroxy proline (387.100), Asparagine and extra derivatives (285.17) conforms to some of the amino acids in blank keratin as reported in the literature. The result of this analysis shows the

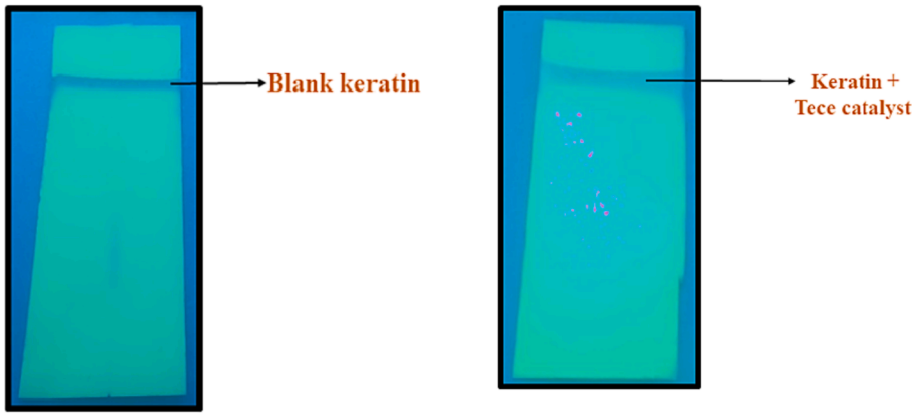

Fig. 10. Thin layer chromatogram of Keratin on light irradiation.

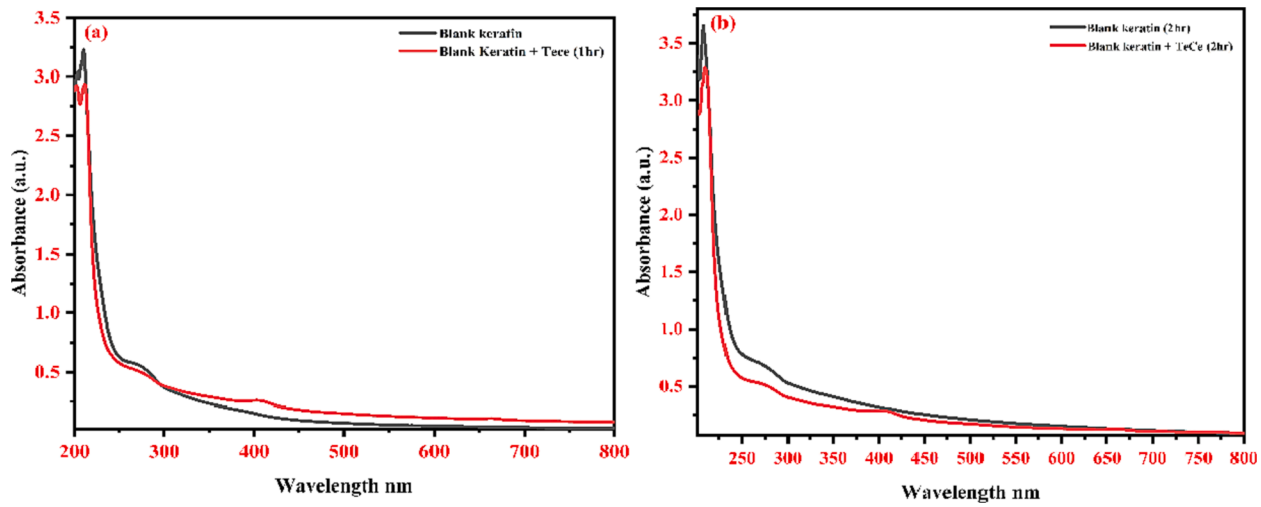

Fig. 11. (a) UV– visible spectrum of blank collagen (b) UV – Visible spectrum of blank collagen with TeCe BNPs after light irradiation.

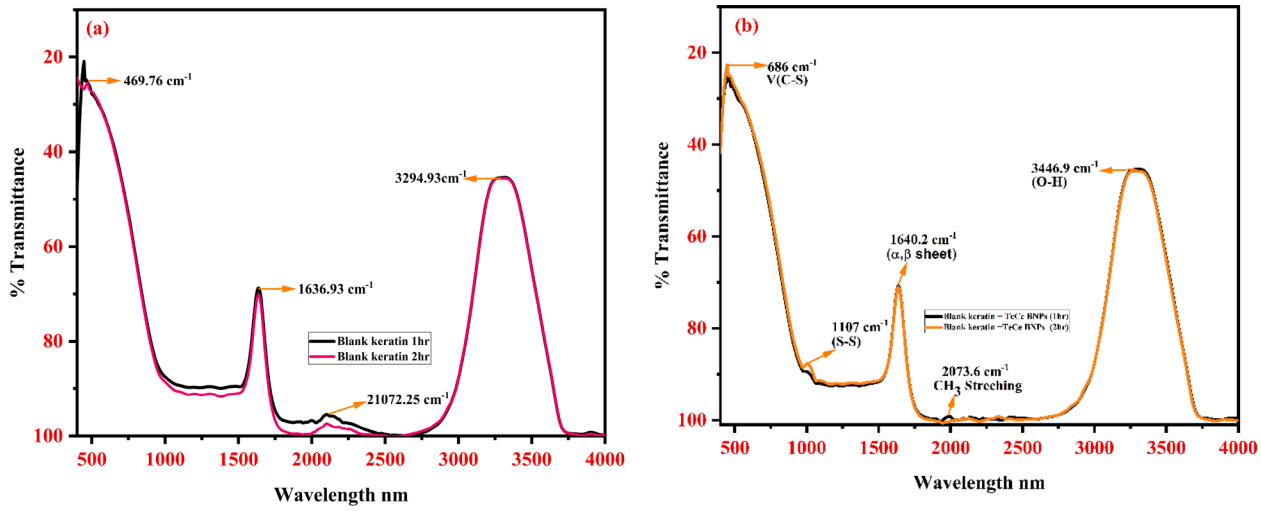

Fig. 12. (a) FTIR spectrum of Blank keratin after 1hr and 2hr irradiation (b) FTIR spectrum of blank keratin with TeCe BNPs after 1hr and 2hr irradiation.

peak of low molecular weight amino acids such as methionine (132.10), Aspartic acid (134.01), Taurine (125.98), Arginine (120.08), Cysteine (Cys + $H^{+)}$ (124.03) after 2hrs of irradiation using Photocatalyst TeCe BNPs, which conforms to the conversion of the polypeptide [32,33].

4.9. Mechanism of keratin degradation

The mechanism involved in keratin degradation will follow a two-step hydrolysis process such as sulfitolysis and proteolysis. In the first stage, the disulfite reductases in little protein would cause a reduction of disulfide bonds and the production of denatured keratin, which could later be decomposed by protease into soluble products (peptides/amino acids). Hence, a breaking of disulfide bonds in keratin will initiate the degradation on light irradiation (2hr) of keratin with TeCe BNPs, which will play a significant role in keratinase formation [34,35].

4.10. Contact angle measurement

Contact angle measurement of catalyst-loaded keratin and blank keratin has been carried out in an inert glass material, which indicates the hydrophilic and hydrophobic behaviour of degraded keratin. The average contact angle (Fig. 17) values for blank keratin and catalyst-loaded keratin at different time intervals are 34.27, 44.84, and 9, 50. 7.45. The increases in contact angle below 60° with increases in irradiation time for catalyst loaded on compared to blank confirms the hydrophilic nature of BNPs. The result visualizes the good adhesive nature of degraded keratin on non – hydrophobic porous surfaces [29]. Table 4 shows the contact angle value of Blank keratin and TeCe-loaded Keratin at different time intervals.

4.11. Electrochemical behaviour of TeCe BNPs

To determine the electrochemical action of keratin on a camphor-mediated TeCe-loaded MGCE electrode, cyclic voltammetry was performed. (Fig. 18) illustrates the cyclic voltammetry of TeCe BNPs on MGCE at dissimilar scan rates 10–100 $MV^{-1}s^{-1}$. The result reveals increases in anodic–cathodic peak current with increases in scan rate to visualize the electrochemical activities of TeCe BNPs. The CV experiment for the determination of electrochemical properties has been carried out using $K[Fe(CN)_6]$ as a redox probe at distinct scan rates 10–100

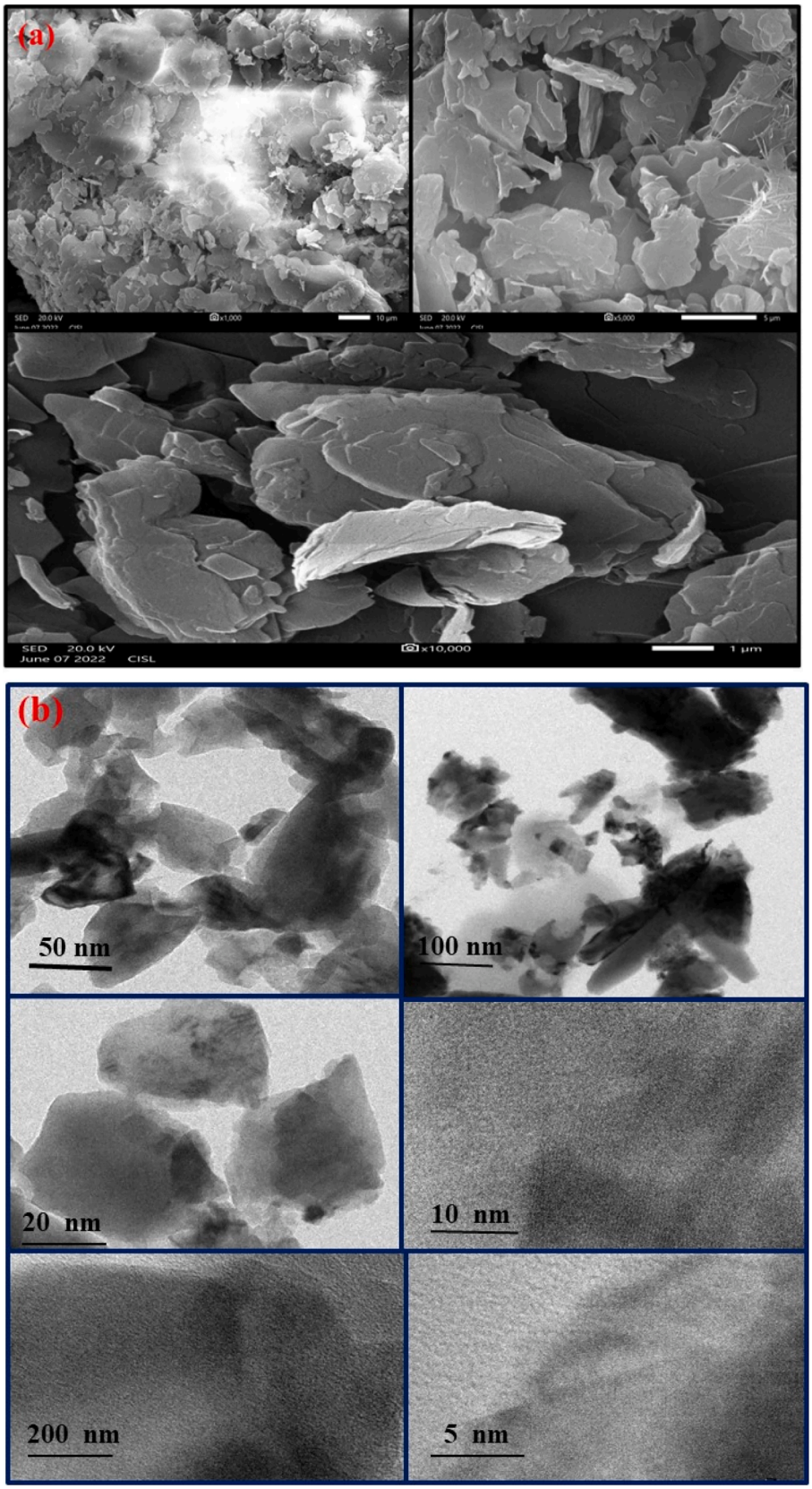

Fig. 13. (a) SEM image of keratin (b) Microscopy image of blank keratin with TeCe BNPs after 2hr irradiation.

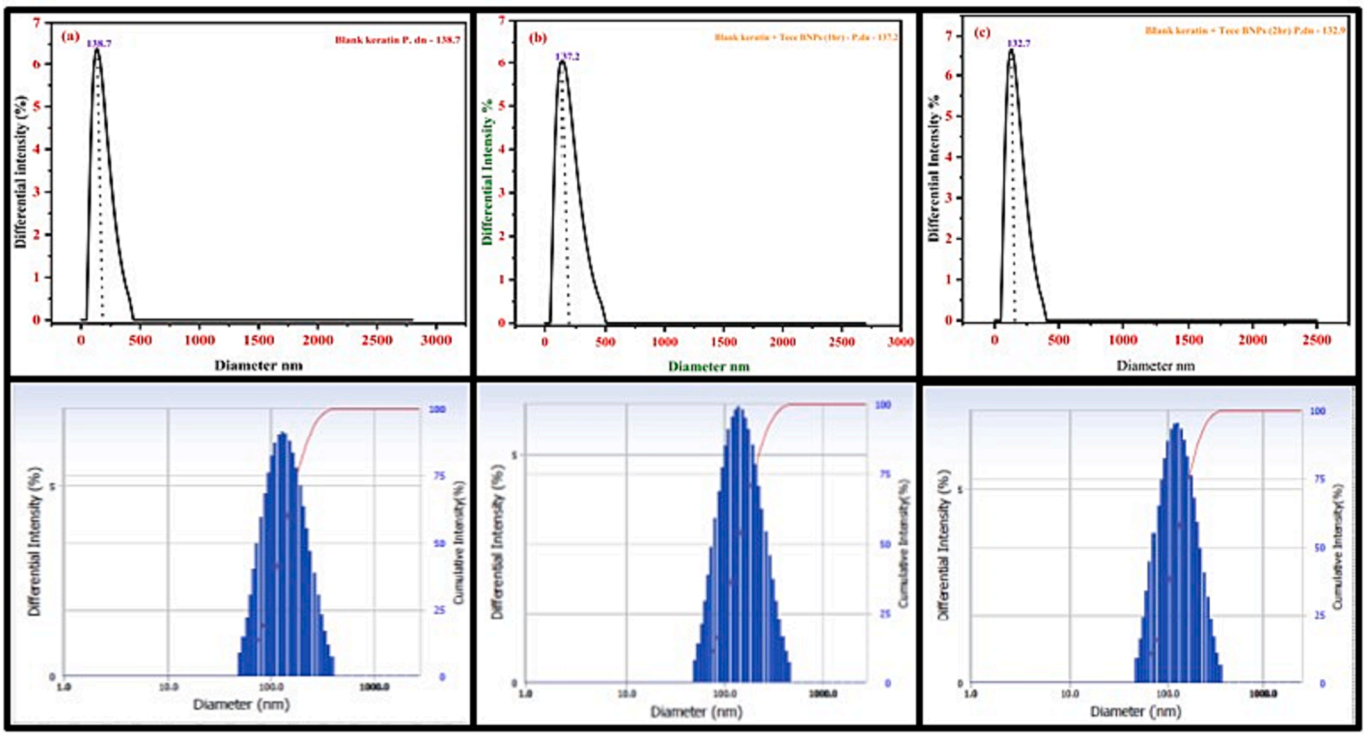

Fig. 14. Depicts the particle size distribution of (a) blank keratin (b) after 1hr (iii) 2 h of irradiation.

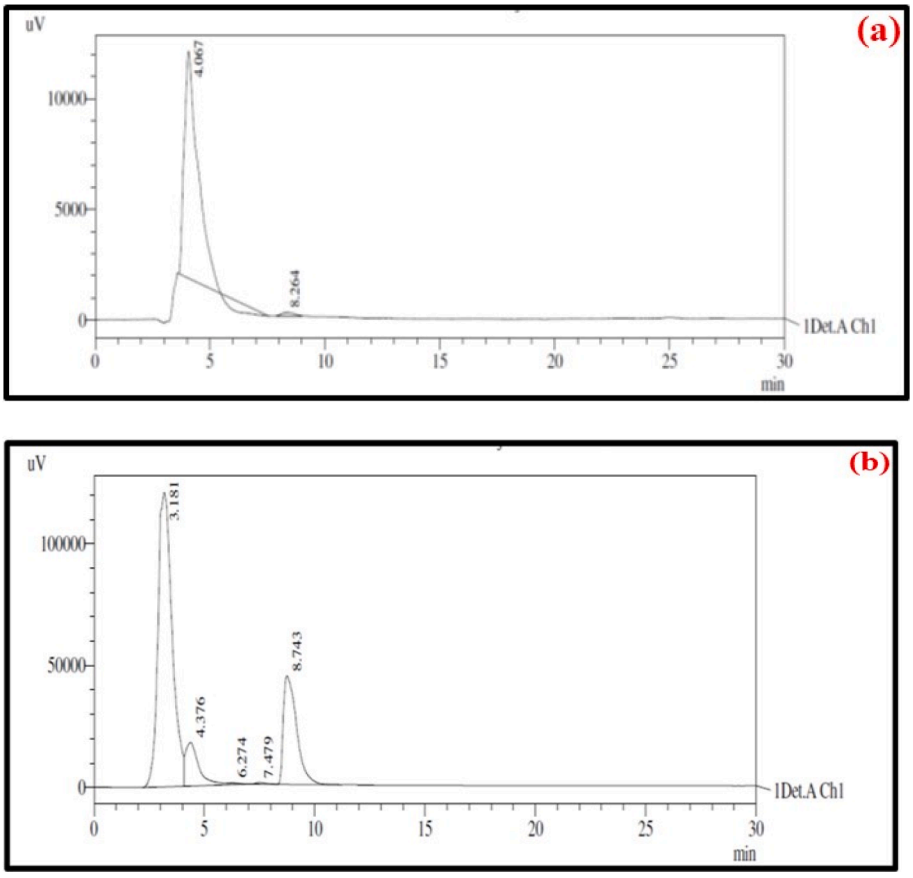

Fig. 15. (a) HPLC Chromatogram of Blank keratin (b) HPLC chromatogram of keratin which was obtained after a 2hr irradiation.

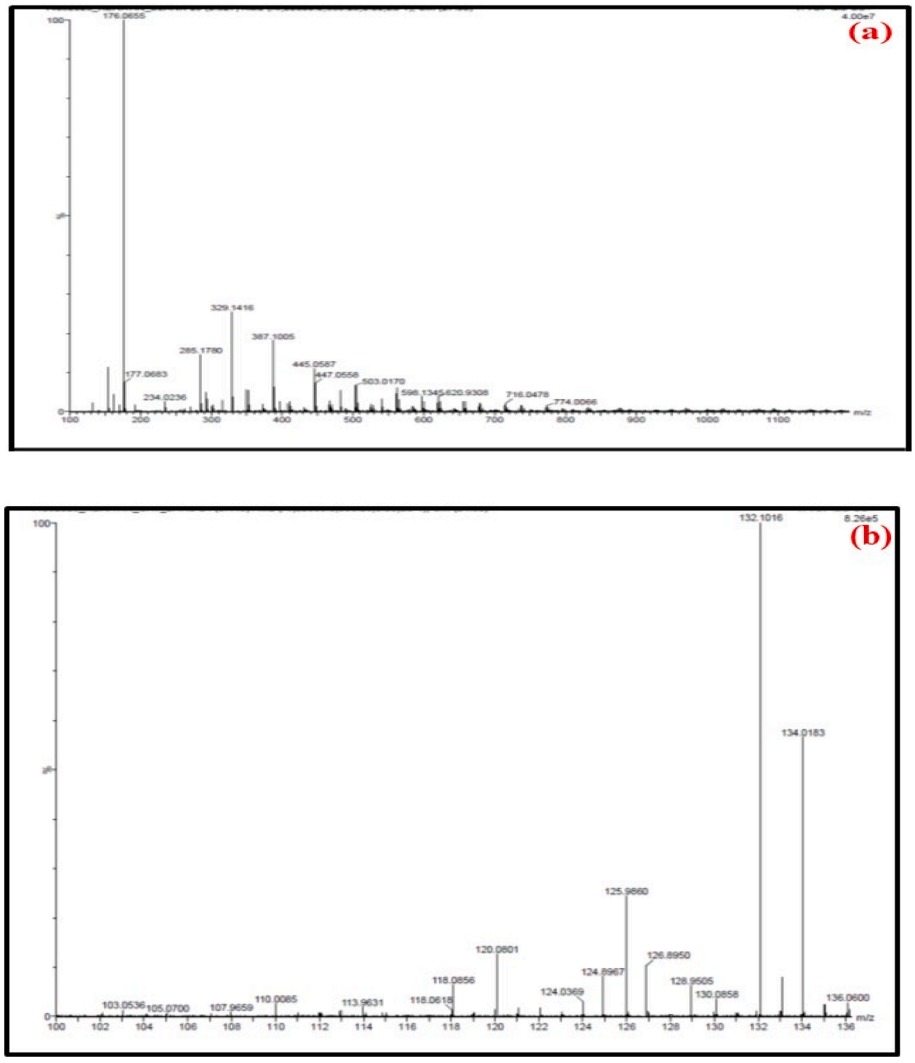

Fig. 16. (a) the HR-mass spectrum of blank keratin and **(b)** the HR-mass spectrum of keratinases product after 2hr light irradiation.

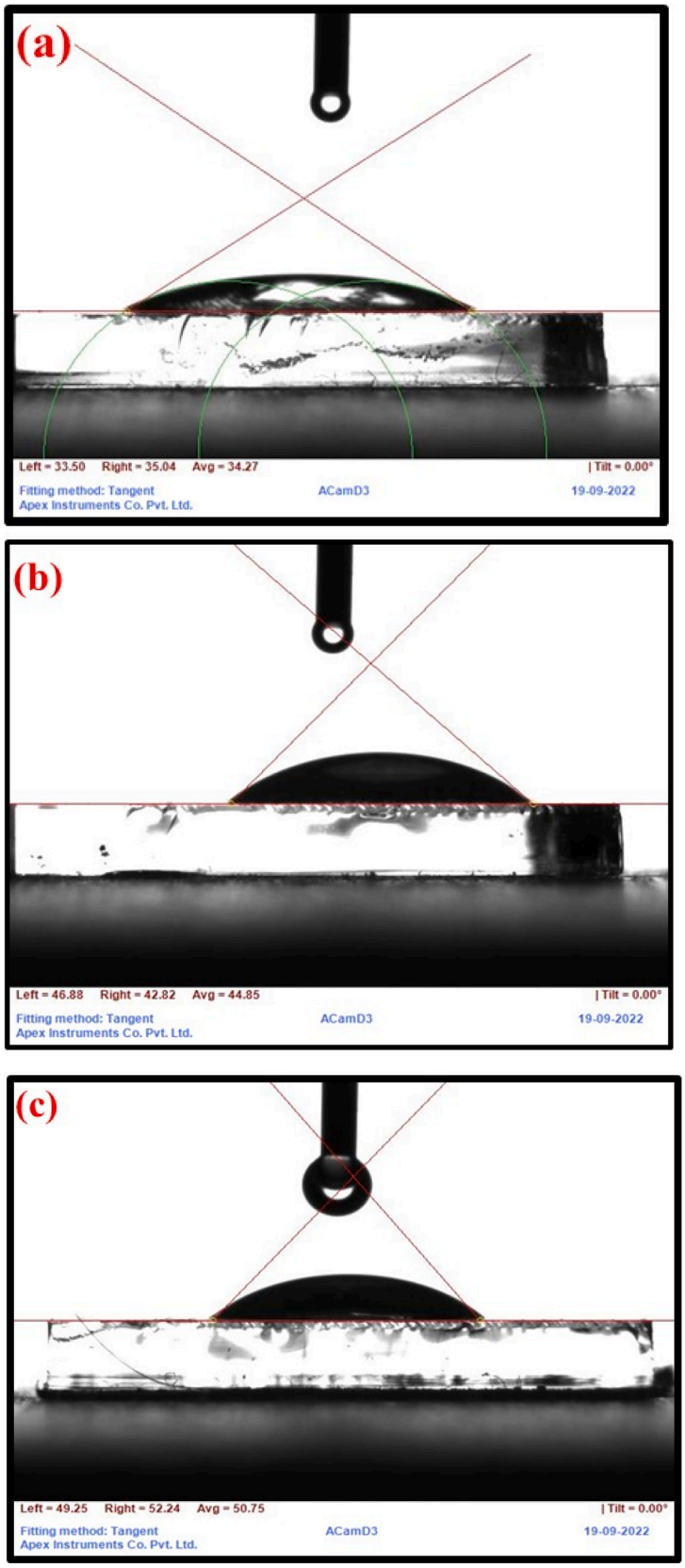

Fig. 17. (a) contact angle measurement of TeCe loaded keratin without irradiation (b) contact angle measurement of UV – irradiated TeCe loaded keratin after time intervals (1hr) (c) contact angle measurement of UV – irradiated TeCe loaded keratin after time intervals (2hr).

Table 4
Contact angle value of Blank keratin and TeCe loaded Keratin at different time intervals.

Contact angle (left)	Contact angle (right)	Average contact angle
33.504	35.036	34.27
46.88	42.818	44.849
49.25	52.24	50.745

MV^{-1} S^{-1}. A linear association between the intermediate peak current and the square root of the scan rate visualizes that the electrochemical process was diffusion-controlled. It is denoted as Ipa = $-3E^{-06}$ X-$6E^{-07}$ (R^2 = 0.9),-9E-05X + 0.2077(R^2) = 0.004 [36]. Table 5 Ipa, Ipc, Epa, Epc values of TeCe BNps at different scan rates.

4.12. Sensing behaviour of TeCe BNPs

Sensing of keratin polypeptide is done with various concentration solutions by cyclic voltammetry using camphora–mediated TeCe loaded MGCE in PBS solution with a 0.1 M solution of K $[Fe(CN)_6]$. Further, it was compared with various analytes (Tryptophan, Methyl uracil, and Uric acid). (Table 6) illustrates the comparative analysis of various analytes in terms of detection limit, linear range, and Sensitivity. Hence, the materials used for electrode preparation are simple; low-cost electrodes are utilized as effective electrodes for sensing keratin. The accuracy of keratin detection was evaluated by the standard addition approach through percent recovery. The recovery rate of the value of various analytes was calibrated from the peak current. The average recovery rate was found to be 99% will indicates excellent recovery. Therefore, the standard addition strategies have been successfully used for keratin determination with appropriate accuracy.LOD and LOQ values were determined from the linear regression investigation and were found to be 0.05, and 0.1 μm respectively. The sensitivity of the electrode was estimated from the slope of the calibration curve using the following equation: sensitivity = Slope/Active surface area [37,38,39]. Table 7 Comparison of various parameters (Sensitivity, LOD, LOQ, Detection limit) of biosensors. Fig. 19. (a) Sensing and reusability curve of various sensing agents (Keratin, uric acid, Methyl uracil, Tryptophan) in different concentrations at a 50MVS^{-1} scan rate (b) reusability curve of various sensing agents (Keratin, uric acid, Methyl uracil, Tryptophan) in different concentrations at a 50MVS^{-1} scan rate. Fig. 20.(a)A linear calibration curve of various sensing agents at different concentrations with an R^2 correlation coefficient (b) A linear calibration curve of various sensing agents after 48 hrs at different concentrations with an R^2 correlation coefficient.

4.13. Selectivity of TeCe BNPs

Selectivity analysis of various analytes such as Tryptophan, uric acid, and methyl uracil was verified using some electrolytes like NaCl, KCl, and CaF_2, and the effect of supporting electrolytes on sensing keratin was studied in the presence of $K[Fe(CN)6]^{-2}$ redox mediator in PBS solution. In the presence of neutral electrolytes KCl, NaCl, and CaF_2 in a 0.1 M concentration solution, no weak current response was observed. However, in the presence of PBS buffer solution with K $[Fe\ (CN)_6]^{-2}$ containing CaF_2, the response of the current towards keratin sensing was significantly enhanced. Table 8 shows the potential of some of the interfering agents with electrolyte-loaded keratin. Hence, as per the result of the current response, 0.1 M PBS solution was selected as the effective supporting electrolyte. Decreases in peak current with or without interfering agents suggest the sensing ability of camphor-mediated TeCe BNPs. The percentage of interference can be predicted using the equation [40].

$$\%\text{interference} = \frac{V_i - V_u}{V_i} \times 100$$

Table 8 shows the potential of some of the interfering agents with electrolyte-loaded keratin.

4.14. Reproducibility and stability of TeCe BNPs

To evaluate the repeatability of the modified electrode, successive measurement was carried out in a 0.03 M solution of keratin at a single *camphor*-mediated TeCe-loaded BNPs after 48 h (Fig. 21a). A four-modified TeCe-loaded MGCE shows increases in peak current with a relative standard deviation (RSD) of 1% for keratin and tryptophan and 4.8. and 8.3% for methyl uracil, and uric acid, respectively. Further, the reproducibility analysis of TeCe-loaded MGCE was predicted by an oxidation peak current of 0.03 M solution of keratin after 48 h. The stability analysis of camphor-mediated TeCe BNPs was estimated by operating at 30 cycles per turn. The increases in peak current with an increment of each cycle per turn up to 30 cycles per turn reveals the stability of BNPs.

5. Conclusion

In the present investigation, the synthesis of TeCe BNPs is carried out using *Cinnamomum camphora* plant extract as a mediator. The synthesized nanoparticles are characterized through various studies, including UV–visible spectroscopy, XRD, SEM-EDX, FTIR, and HR-TEM. The degradation of biochemical contaminants using *Cinnamomum camphora*-mediated TeCe BNPs is investigated. The average particle size of the TeCe BNPs is measured to be 103 nm with a zeta potential (ZP) value of 0.3 mV is found to be greater compared to other studies such as AFM and HR-TEM. This indicates a higher stability and dispersive nature, thereby confirming the hydrodynamic coating of BNPs. The surface area of TeCe BNPs is determined to be 1.3, with a pore diameter of 1.088 and a pore volume of 3.0948, revealing the catalytic activity of the nanoparticles. Furthermore, the degradation of biochemical contaminants, specifically keratin, is conducted using *Cinnamomum camphora*-mediated TeCe BNPs. The sensing behaviour is analyzed using keratin analytes and compared with various other substances, including tryptophan, methyl uracil, and uric acid.

CRediT authorship contribution statement

M. Sindhu Devi: Data curation, Formal analysis, Methodology, Writing – original draft. **A. Muthuvel:** Methodology, Writing – original draft. **S. Srinivasan:** Methodology, Project administration, Data curation, Supervision, Writing – review & editing. **Abeer A. AlObaid:** Writing – review & editing. **Ismail Warad:** Writing – review & editing. **Basheer M. Al-Maswari:** Writing – review & editing.

Declaration of Competing Interest

The authors declare that they have no known competing financial interests or personal relationships that could have appeared to influence the work reported in this paper.

Data availability

Data will be made available on request.

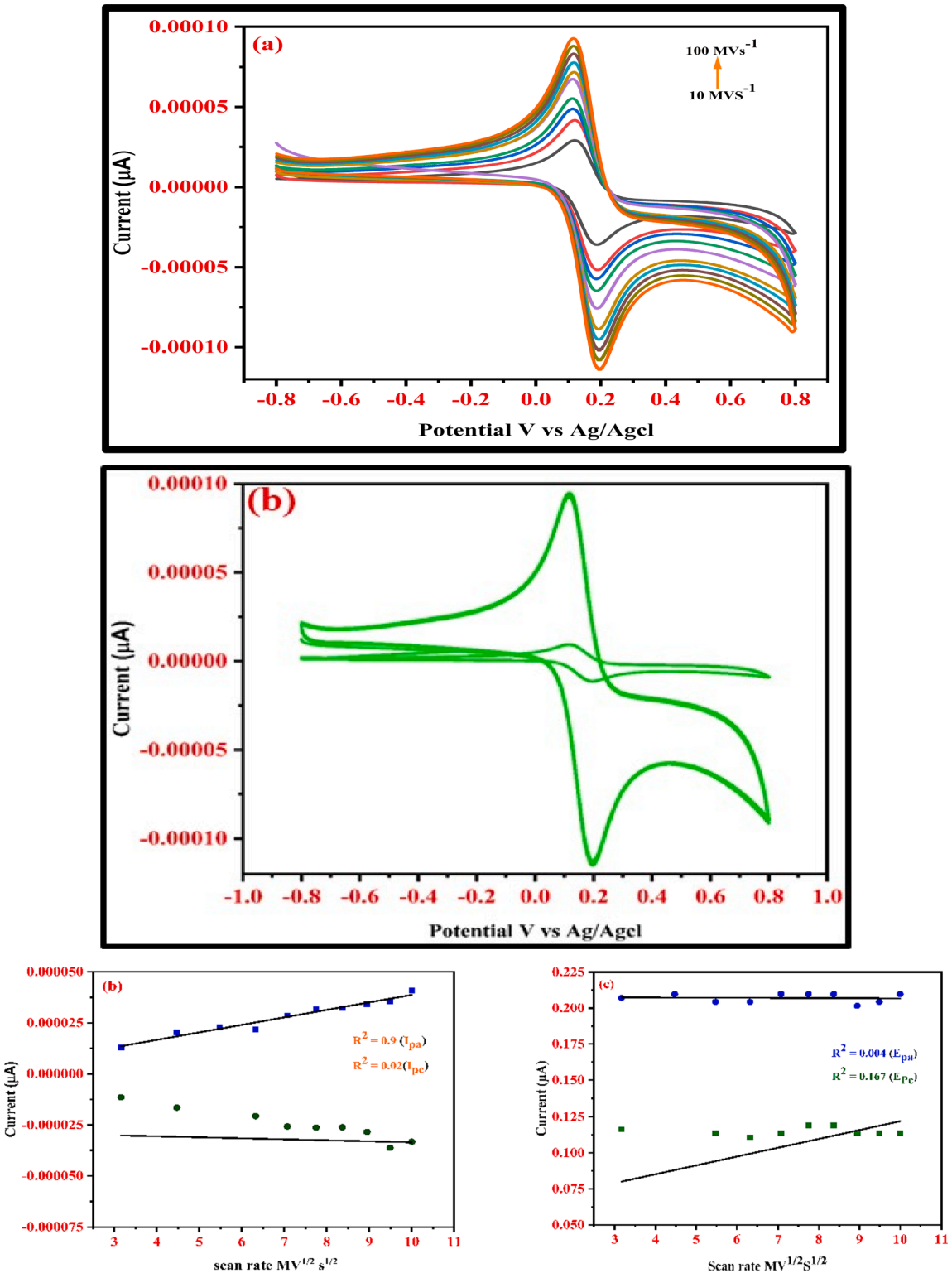

Fig. 18. (a)Cyclic voltammetry of TeCe BNPs at different scan rates of 10 MVs^{-1} to 80Mvs^{-1}(b) A linear calibration curve of (I_{pa}, I_{pc}) vs square root of scan rate (c) A linear calibration curve of anodic and cathodic peak current vs the square root of scan rate (E_{pa} and E_{pc}).Table 5 I_{pa}, I_{pc}, E_{pa}, E_{pc} values of TeCe BNPs at different scan rates.

Table 5
Ipa, Ipc, Epa, Epc values of TeCe BNPs at different scan rates.

Scan rate $MV^{1/2}$ $S^{1/2}$	The square root of the scan rate $MV^{1/2}S^{1/2}$	I_{PC}	I_{Pa}	E_{Pa}	E_{pc}
10	3.16227766	−0.00001145	0.000012948	0.11627	0.20702
20	4.472135955	−1.64964E-05	0.000020419	0.119015	0.20975
30	5.477225575	−0.00001751	0.000022807	0.113543	0.20428
40	6.32455532	−0.000020713	2.17318E-05	0.110807	0.204286
50	7.071067812	−0.000025784	0.00002867	0.113543	0.209758
60	7.745966692	−0.00002626	0.000031692	0.11901	0.209758
70	8.366600265	−0.000026146	3.22071E-05	0.11901	0.209758
80	8.94427191	−2.83955E-05	3.41248E-05	0.11354	0.20155
90	9.486832981	−0.000036219	3.53707E-05	0.11354	0.20428
100	10	−0.000033227	4.07744E-05	0.11354	0.20975

Table 6
Comparison of sensitivity with LOD and LOQ value for sensing agent with variously reported novel catalyst.

Biosensor	Substrate	LOD	LOQ	Detection limit	Sensitivity	Linear range	References
TeCe	Keratin	0.0562924	0.1705831	4.90E-04	0.005859	−1.9	Current work
TeCe	Uric acid	0.040489	0.122695	5.97E-04	0.00098284	−1.992	Current work
TeCe	Methyl uracil	0.019037	0.057689	4.71E-04	−0.0065787	−2	Current work
TeCe	Tryptophan	0.0427173	0.1294465	5.78E-04	0.01088	−1.9	Current work
nHA/CPE	Uric acid	–	–	0.05	–	–	[37]
Graphite electrode	L –Tryptophan	1.73	5.78	5.0–150.0	–	–	[38]
UOX/FC/CU2O/GCE	Uric acid	0.0596	–	0.01 −1mM	1.9	–	[39]

Table 7
Comparison of various parameters (Sensitivity, LOD, LOQ, Detection limit) of biosensors.

Substrate	LOD	LOQ	Detection limit	Sensitivity	Linear range
Keratin	0.076937	0.23314		0.010474	−0.9–1.0
Uric acid	0.00489	0.007409	5.93E-06	0.049887	−1.0–0.992
Methyluracil	0.069235	0.209805	3.69E-04	0.00694	−1.995
Tryptophan	0.024983	0.075706	1.96E-04	0.011537	−0.9815–0.994

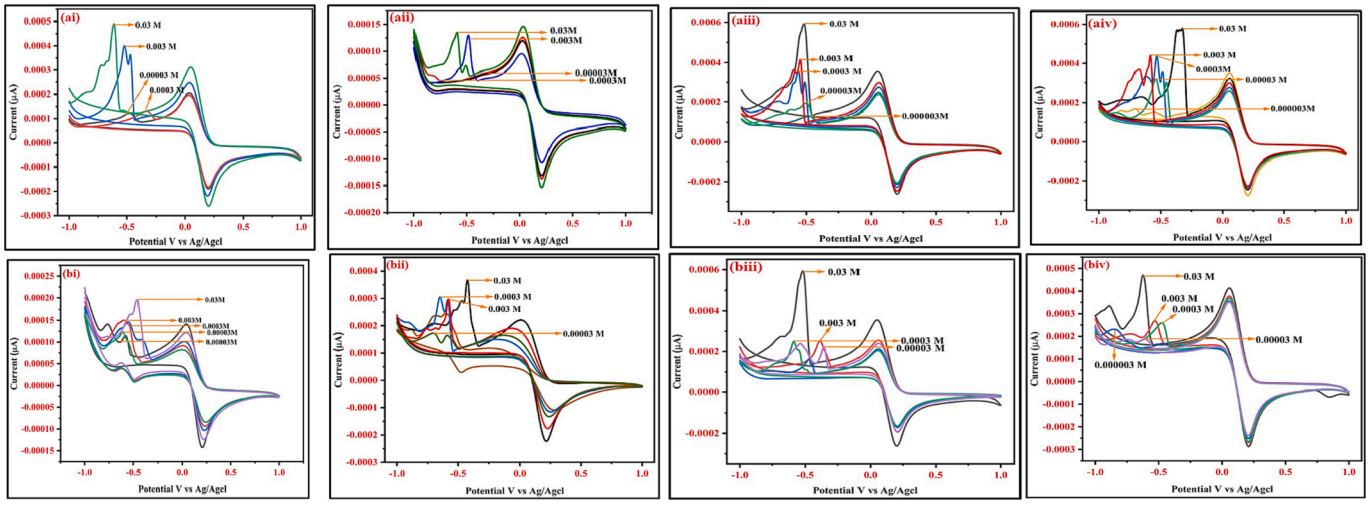

Fig. 19. A(i)sensing curve of various sensing agents (i) keratin(ii) uric acid (iii)methyl uracil (iv)tryptophan in different concentrations at a 50mvs^{-1} scan rate (ii) reusability curve of various sensing agents (i)Keratin(ii) uric acid(iii)Methyl uracil (iv)Tryptophan in different concentrations at a 50MVS^{-1} scan rate.

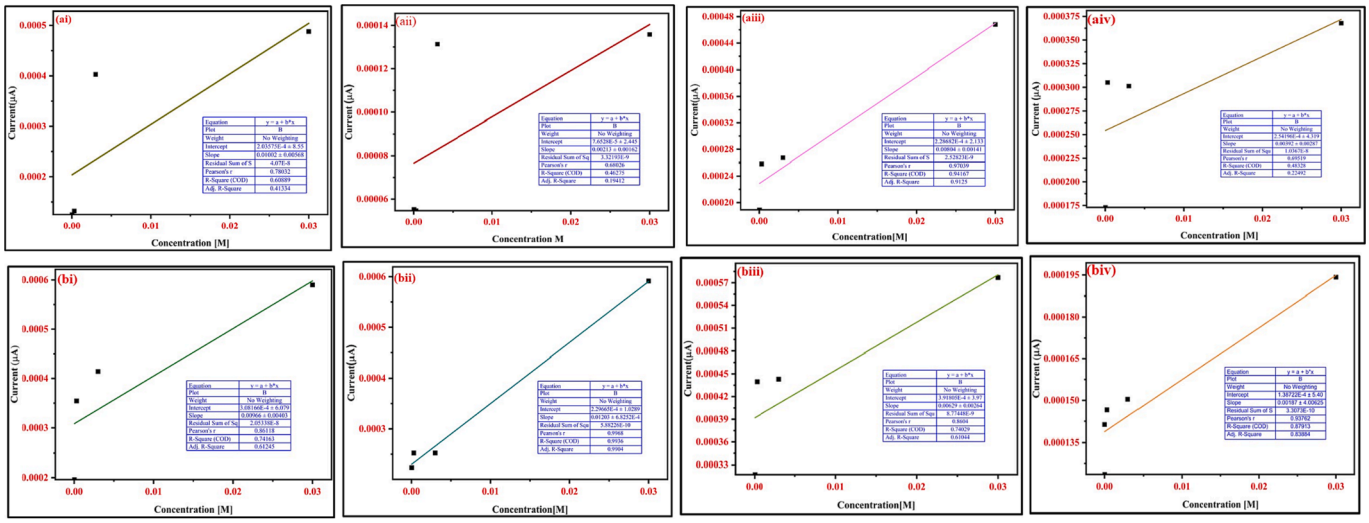

Fig. 20. a(i) A linear calibration curve of various sensing agents(i) Keratin(ii) uric acid (iii)Methyl uracil (iv)Tryptophan at different concentrations with an R^2 correlation coefficient (ii) A linear calibration curve of various sensing agents (i) Keratin(ii) uric acid (iii)Methyl uracil (iv)Tryptophan on after 48 h at different concentrations with an R^2 correlation coefficient.

Table 8
The potential of some of the interfering agents with electrolyte-loaded keratin.

Some of the interfering agents with electrolyte	Voltage Mv
Keratin	0.01332
Keratin + CaF_2	0.3297
Keratin + KCl	0.21553
Keratin + NaCl	0.12689

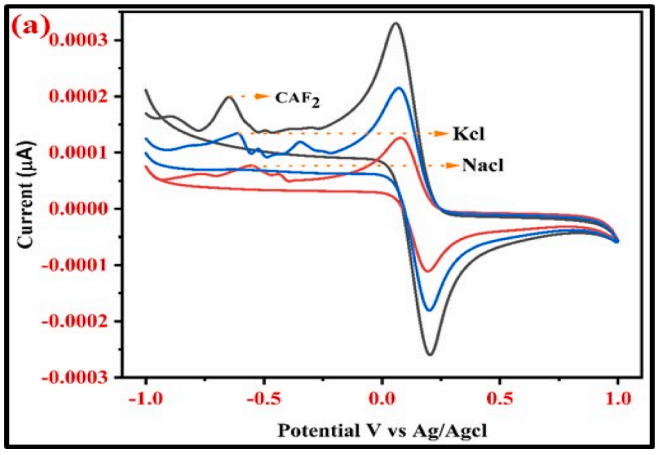

Fig. 21. (c) Cyclic voltammetry of TeCe BNPs on sensing Keratin in the presence of an interfering agent.

Acknowledgments

The authors extend their appreciation to the Researchers Supporting Project number (RSP2023R381), King Saud University, Riyadh, Saudi Arabia

References

[1] W.S. Tung, W.A. Daoud, Photocatalytic self-cleaning keratins: A feasibility study, Acta Biomater. 5 (2009) 50–56.
[2] T.K. Kumawat, A. Sharma, V. Sharma, S. Chandra, Keratin waste: the biodegradation polymers, INTECH open.9 (2018) 1–22.
[3] J. Qiu, CWilkens, K. Barrett, A.S. Meyer, Microbial enzymes catalyzing keratin degradation: classification, structure Function, Biotechnol Adv. 44 (107607) (2020) 1–22.
[4] K. Teresasa, B. Justyna, Biodegradation of keratin waste: theory and practical aspects, Waste Manage. 31 (2011) 1689–1701.
[5] M. Brebu, L. Spiridon, Thermal degradation of keratin waste, J. Anal. Appl. Pyrol. 91 (2011) 288–295.
[6] A.R. Birari, K.P. Narkhede, R.C. Salunkhe, Feather keratin degradation by stenotrophomonas Sp.AB20 screened from poultry waste, J. Pure Appl. Microbiol. 7 (4) (2013) 2973–2979.
[7] J.S. Church, K.R. Millington, Photodegradation of wool keratin: part I vibrational spectroscopic studies, Biospectroscopy 2 (1996) 249–258.
[8] K.R. Millington, J.S. Church, The photodegradation of wool keratin II proposed mechanism involving cysteine, J. Photochem. Photobiol. B Biol. 39 (1997) 204–212.
[9] D.D. Shah, J. Zhang, H. Maity, K.M.G. Mallela, Effects of photodegradation on the structure, stability, aggregation, and function of an IgG, Monoclonal antibody, Int. J. Pharm. (2018) 1–48.
[10] B. Gandhe, K. Anguluri, S. Bodhankar, S.S.K.P. Vurukonda, Microbial degradation of keratin and its agro-industrial prospective applications, Int. J. Current Adv. Res. 7 (2018) 9709–9716.
[11] R. Quertani, H. Chouchane, M. Mahjoubi, H. Khdhira, A.S. Masmoudi, A. Cherif, M. Neifar, Feather degradation efficiency and hide dehairing ability of a new keratinolytic bacillus halotolerant strains, isolated from a tannery wastewater, Appl. Bionics Biomech. 4 (5) (2020) 102–110.
[12] M. Calin, D. ConstantinescuAruxandei, E. Alexanndrescu, l. Raut, M. BadeaDoni, M. Arsene, F. Oancea, L. Jecu, V. Lazar, Degradation of keratin substrates by keratinolytic fungi, Electronic J. Biotechnol. 28 (2017) 101–112.
[13] Z. Peng, X. Mao, J. Zhang, G. Du and J. Chen, Biotransformation of keratin waste to amino acids and achieve peptides based on cell-free catalysis, Biotechnol. Biofuels.13:61 (2020)1-12.
[14] A. Gousterova, D. Braikova, I. Goshev, P. Christov, K. Tishinov, E. Vasileva-Tonkova, T. Haertle, P. Nedkov, Degradation of keratin and collagen containing wastes by newly isolated thermoactinomycetes or by alkaline hydrolysis, Lett. Appl. Microbiol. 40 (2005) 335–340.
[15] A. Jaitovich, S. Mehta, N. Na, A. Ciechanover, R.D. Goldman, K.M. Ridge, Ubiquitin – Proteasome mediated degradation of keratin intermediated filaments in mechanically stimulated A549 cells, J. Biol. Chem. 283 (2008) 25348–25355.
[16] P. Nasipuri, J. Herschend, A.D. Brejnrod, J.S. Madsen, R. Espersen, B. Svensson, S. Mette Burmolle, S.J.S. Jacquiod, Community intrinsic properties enhance keratin degradation from bacterial consortia, Plos One 15 (1) (2020) 1–26.
[17] M. Sharma, M. Sharma, V.M. Rao, In vitro biodegradation of keratin by dermatophytes and some soil keratinophilic, African J. Biochem. Res. 5 (1) (2011) 1–6.
[18] M. Sindhudevi, B. Karthikeyan, G. Gnanamoorthy[b], S. Srinivasan, Green synthesis of core-shell Te-se bimetallic nanoparticles using their Cinnamomum camphora leaf extract and their invitro cholesterol degradation,128:112375 (2020)1-15.
[19] A. Amari, M.K. Almesfer, N.S. Alsaiari, M. Danish, A.M. Alshahrani, M.A. Tahoon, F.B. Rabah, Electrochemical and optical properties of tellurium dioxide (TeO2) nanoparticles, J. Electro. Chem. Sci. 16 (2021) 1–11.
[20] R. Mirjani, M.A. Faramarzi, M. Sharifzadeh, N. Setayesh, M.R. Khoshayand, A. Shahverdi, Biosynthesis of tellurium nanoparticles by lactobacillus plantarum and the effect of nanoparticle – enriched probiotics on the lipid profiles of mice, IET Nanobiotechnol. 9 (2015) 300–305.

[21] A. Miri, M. Darroudi, M. Sarani, Biosynthesis of cerium oxide nanoparticles and its cytotoxicity survey against colon cancer cell line. Appl. Organomet. Chem. e5308 (2019)1-7.
[22] E. Kumar, P. Selvarajan, K. Bala Subramanian, Preparation and studies of cerium dioxide(CeO2) nanoparticles by microwave assisted solution method, Recent Res. Sci. Technol. 2 (4) (2010) 37–41.
[23] J. Huang, Q. Li, D. Sun, Y. Lu, Y. Su, X. Yang, H. Wang, Y. Wang, W. Shao, N. He, J. Hong, C. Chen, Biosynthesis of silver and gold nanoparticles by novel sundried cinnamomum camphora leaf, Nano Technol 18 (2007) 1–12.
[24] G. Guisbiers, L.C. Mimum, R. Mendoza–cruz, K.L. Nash, Synthesis of tunable tellurium nanoparticles, Semi. Cond. Sci. Technol. 32(2017)1-6.
[25] K. Siposova,V. Huntosova, Y. Shlapa, L. Lenkavska, M. Macajova, A. Belousand, A. Musatov, Advanced in the study of cerium oxide nanoparticles: New Insights into antiamyloidogenic activity, ACS Appl. Bio. Mater. 2(2019) 1884-1896.
[26] E. Beche, P. Charvin, D. Perarnau, S. Abanades, G. Flamant, Ce 3d XPS investigation of cerium oxides and mixed cerium oxide (CeTiYO2), Surf. Interface Anal. 40 (2008) 264–267.
[27] V. Shah, S. Shah, H. Shah, F.J. Rispoli, K.T. McDonnell, S. Workeneh, A. Karakoti, A. Kumar, S. Seal, Antibacterial activity of polymer coated cerium oxide nanoparticles, Plosone. 7(2012)1-14.
[28] P. Tamizhdurai, S. Sakthinathan, S.M. Chen, K. Shanthi, S. Sivasanker, P. Sangeetha, Environmentally friendly synthesis of CeO2 nanoparticles for the catalytic oxidation of benzyl alcohol to benzaldehyde and selective detection of nitrite, Sci Re. 7 (1) (2017) 46372.
[29] Mihaela –Doinani Culescu, Mariana Daniela Berechet, Carmen Gaidau, Madalina Ignat, Mihai Radu, Study on obtaining keratin extracts from leather industries by-products, in: 6th international conference on advanced materials and Systems. (2016) 1-6.
[30] N.W. Ge, Y. Zhang, H. Zhang, L. Cheng, X. P. Shi, Extraction and characterization of keratin and keratin hydrogels from wasted rabbit hair, J. Physics:Conference Series.1790 (2020)1-8.
[31] X. Wang, Z. Shi, Q. Zhao, Y. Yun, Study on the structure and properties of biofunctional keratin from rabbit hair, Materials. 14 (2021) 1–16.
[32] M. Brebu, L. Spiridon, Thermal degradation of keratin waste, J. Anal. Appl. Pyrol. 91 (2011) 288–295.
[33] K.K. Stenerson, The Derivatization and analysis of aminoacids by GC-Ms.25.3 (2023)1-6.
[34] Z. Peng, X. Mao, J. Zhang, G. Du, J. Chen, Biotransformation of keratin waste to aminoacids and active peptides based on cell – free catalysis, Biotechnology Biofuels.13:61(2020) 1-13.
[35] B. Gandhe, K. Anguluri, S. Bodhankar, S.S.K.P. Vuru konda, Microbial degradation of keratin and its Agro–industrial prospective Application, Int. J. Curr. Adv. Res. 7 (2018)9709–9716.
[36] Q. He, J. Liu, J. Feng, Y. Wu, Y. Tian, G. Li, D. Chen, Sensitive voltammetric sensor for tryptophan detection by using polyvinylpyrrolidone functionalized graphene/GCE, Nanomaterials 10(1)125 (2020) 1–16.
[37] E. Iyyappan, S.J. Samuel Justin, P. Wilson, A. Palaniappan, Nanoscale hydroxyapatite for electrochemical sensing of uric acid: Roles of mesopore volume and surface Acidity. ACS Appl.Nanomater. 3(2020)7761-7773.
[38] Z.Z. Tasic, M.B.P. Mihajlovic, M.B. Radovanovic, A.T. Simonovic, D.V. Medic, M.M. Antonijevic, Electrochemical determination of L- Tryptophan in food samples on graphite electrode prepared from waste batteries, Scientific Rep. 12:5469 (2022) 1-11.
[39] Q. Yan, N. Zhi, L. Yang, G. Xu, Q. Feng, Q. Zhang, S. Sun, A highly sensitive uric acid electrochemical biosensor based on a nano-cube cuprous oxide/ferrocene/uricase modified glassy carbon electrode, Scientific Rep.10:10607 (2020)1-10.
[40] C.S. Kushwaha, P. Singh, S.K. Shukla, G.C. Dubey, Electrochemical urea sensing over polyaniline grafted chitosan copolymer, Mater. Today Proc. 5 (2018) 15253–15260.